To the Graduate Council:

I am submitting herewith a thesis written by Irene Elizabeth Paulauskas entitled "Polarization Studies of Thermally Grown Chromium Nitrides for Possible Applications in Polymer Electrolyte Membrane Fuel Cells". I have examined the final paper copy of this thesis for form and content and recommended that it be accepted in partial fulfillment of the requirements for the degree of Master of Science, with a major in Materials Science and Engineering.

R. A. Buchanan

Dr. Raymond A. Buchanan,
Major Professor

We have read this thesis and recommended its acceptance:

Dr. Michael P. Brady

Charles S. Feigerle

Dr. Charles S. Feigerle

Accepted for the Council:

Vice Provost and Dean of Graduate Studies

Thesis
P385

Polarization Studies of Thermally Grown Chromium Nitrides for Possible Applications in Polymer Electrolyte Membrane Fuel Cells

A Thesis Presented for the
Master of Science Degree
The University of Tennessee, Knoxville

Irene Elizabeth Paulauskas
December 2003

DEDICATION

This thesis is dedicated to my parents, Alfonso Paulauskas and Regina Vasaitis de Paulauskas, and my sister, Regina Paulauskas, for their love, sacrifices, values and beliefs; all my achievements are also theirs. It also is dedicated to Beba, for all the good and bad times, and the rest of my family, especially to my grandparents for all their support and laughs.

ACKNOWLEDGEMENTS

I would like to thank my two advisors, Drs. Ray Buchanan and Michael Brady; their guidance, time and endless patience have given me the opportunity to work in a very exciting field.

I greatly appreciate the technical support of Dr. Harry Meyer III, Mr. Larry Walker and Mrs. Dorothy Coffey of ORNL; their expertise helped to developed areas of my research that I did not have the knowledge and experience to understand by my own.

I would like to thank Mr. Doug Fielden and Mr. Yan Cui of the University of Tennessee for all their help on the sample preparation process for the polarization studies.

I would like to thank my fellow graduate reseach group. They gave me great insights in the lab as well as in our regular meetings. Special gratitude is given to Mr. William Peter for all his help and patience in the corrosion lab.

I am also very greatful to the United States Department of Energy, Energy Efficiency and Renewable Energy, Office of Transportation Technology, which funded this research. This program was thruogh the Oak Ridge National Laboratory (operated by UT-Battelle, LLC, for the U.S. Department of Energy under contract DE-AC05-00OR22725) and was managed by Dr. Michael Brady.

ABSTRACT

Fuel cells can offer near-zero emission power generation at high efficiencies by using the chemical energy of a fuel to produce electrical energy. However, improvement on the materials used in the fabrication of these devices is necessary. In the polymer electrolyte membrane fuel cells (PEMFC) the particularly aggressive environment limits considerably the materials selection. The bipolar plates are responsible for electrical contact among the cells, and at the same time, they guide the reaction gases and products as they enter and leave the cells. Thick graphite plates (with low power densities) are the most commonly used material for this application. Research has been focused on metals, which offer higher electrical and thermal conductivities and better mechanical properties than graphite. However, several authors have reported decreases in the process efficiency due to the formation of resistive surface oxide layers on the plates; as well as, metal-ion contamination on the polymeric membrane[5,6].

The use of protective coatings, such as thermally grown metal nitrides (e.g. Cr_2N), can help to overcome this problem[2,9]. Recent work has demonstrated that thermally grown Cr-nitrides on Ni-Cr base alloys show promise as a means to protect metallic bipolar plates[7]. In support of this premise, the corrosion protection obtained by different nitridation conditions of the Ni-50Cr (wt%) system was studied in more detail. Results suggest that the corrosion resistance increases with the nitridation temperature, and this change is related to the different phases and morphologies obtained. The nitrides seem to be fairly stable at voltages on the order of 750 mV(SHE). Even though a single and uniform phase after nitridation has not been obtained at this point, results seem to imply that a mixture of $CrN+Cr_2N$ gives better corrosion protection in aerated sulfuric acid solution (pH 3 at 80 °C) than that observed with a mixture of Cr_2N and π phase. Polarization behavior observed in a hydrogen purged environment showed that both mixtures ($CrN+Cr_2N$ and $Cr_2N+\pi$ phase) presented low corrosion currents (below $1x10^{-6}$ A/cm^2) in this electrolyte. Preliminary XPS analysis suggests that the current densities measured in the aerated environment are at least partially due to oxygen incorporation into/at the nitride layer. Details of the nitridation conditions, corrosion behavior and microstructure are presented.

TABLE OF CONTENTS

CHAPTER		PAGE
1	Introduction	1
2	Importance of this Research	3
3	Review of Related Literature	4
	3.1. Fuel Cells. General Concepts. Different Types of Fuel Cells	4
	3.1.1. Polymer Electrolyte Membrane Fuel Cells	5
	3.1.1.1. The Polymer Membrane	5
	3.1.1.2. The Catalyst	6
	3.1.1.3. The Electrodes	6
	3.1.1.4 The Bipolar Plates	7
	3.2. Electrochemical Corrosion	7
	3.3. Nickel and Nickel-Chromium Alloys	9
	3.4. Oxidation of Metals	9
	3.5. Nitridation of Nickel-Chromium Alloys	11
	3.6. Corrosion Behavior of Chromium Nitrides	13
4	Experimental Methods	15
	4.1. Sample Fabrication and Preparation	15
	4.2. Heat Treatment	15
	4.3. Sample Characterization	15
	4.4. Corrosion Behavior	15
5	Results and Discussion	17
	5.1. Polarization Tests	17
	5.1.1. First Approach	17
	5.1.2. Nitrided Nickel - Chromium Alloy	17
	5.1.3. Pure Chromium	18
	5.2. Protective Quality	19
	5.3 Dearated Electrolyte	19
	5.4 Correlation with Nitride Microstructure	20
	5.5. XPS Studies	21
6	Conclusions	24
7	Further Research	26
	References	27
	Apendix	31
	Vita	46

LIST OF TABLES

TABLE		PAGE
A.1.	Comparison of Five Fuel Cell Technologies	32
A.2.	PEM Fuel Cell Operating Conditions for Bipolar Plate Materials Design	32

LIST OF FIGURES

FIGURE		PAGE
A.1.	Fuel Cell Basic Operation	33
A.2.	Schematic Diagram Showing the Components of a Polymer Electrolyte Membrane Fuel Cell	33
A.3.	Schematic Diagram of Three Polymer Electrolyte Membrane Fuel Cells Stacked in Series	34
A.4.	Anodic Polarization Curve of an Active - Passive Material	34
A.5.	Nickel Chromium Phase Equilibrium Diagram	35
A.6.	Anodic Polarization Curves of Different Nitrided Alloys	35
A.7.	Ni-50Cr Anodic Polarization Curves. Effect of Temperature and Timing on Nitridation in a Pure Nitrogen Atmosphere	36
A.8.	Effect of Alloy Composition on Nitridation at 1100 °C for 2 h in a Pure Nitrogen Atmosphere	36
A.9.	Effect of the Nitrogen Partial Pressure. Ni-50Cr Anodic Polarization Curves. Pure Nitrogen and Ar-10%N_2 at 1100 °C for 2 h	37
A.10.	Polarization Curves of Pure Chromium. Uncoated and Nitrided at 1100 °C for 2 h	37
A.11.	Protective Quality at 1100 mV (SHE) for the Ni-35Cr and Ni-45Cr Nitrided at 1100 °C for 2 h in Pure Nitrogen	38
A.12.	Protective Quality at 750 mV (SHE) fot the Ni-35Cr and Ni-50Cr Nitrided at 1100 °C for 1 h in Pure Nitrogen	38
A.13.	Polarization Curves in Deaerated Electrolyte of Nitrided Ni-50Cr Alloys at 1100 °C in Pure N_2 and Ar-10%N_2 for 2 h and 5 h Respectively	39
A.14.	Cross Sectional Microstructure of Ni-35Cr Coupon Nitrided at 1100 °C for 2 h in Pure Nitrogen	39
A.15.	Cross Sectional Microstructure of Ni-45Cr Coupon Nitrided at 1100 °C for 2 h in Pure Nitrogen	40
A.16.	Cross Sectional Microstructure after Polarization Test of Ni-50Cr Coupon Nitrided at 875 °C for 30 h in Pure Nitrogen	40
A.17.	Cross Sectional Microstructure after Polarization Test of Ni-50Cr Coupon Nitrided at 1100 °C for 1 h in Pure Nitrogen	41
A.18.	Cross Sectional Microstructure after Polarization Test of Ni-50Cr Coupon Nitrided at 1100 °C for 2 h in Ar-10%N_2	41
A.19.	Concentration Profile of Ni-50Cr Coupon Surface Nitrided at 1100 °C for 2 h in Pure N_2, without Polarization Testing ("as nitrided")	42

A.20. Evolution of the Oxygen, Nitrogen and Chromium Peaks Throughout Sputter of "as nitrided" Ni-50Cr Coupon..... 42
A.21. Concentration Profile of the Polarized Ni-50Cr Coupon Surface (Nitrided at 1100 °C for 2 h in Pure N_2) Hold at 1000 mV(SHE) for 5 h..... 43
A.22. Evolution of the Oxygen, Nitrogen and Chromium Peaks Throughout Sputter of the Polarized Ni-50Cr Coupon Surface (Nitrided at 1100 °C for 2 h in Pure N_2) Hold at 1000 mV(SHE) for 5 h 43
A.23. Comparison of the Chromium Peaks after Final Sputter for the Ni-50Cr Nitrided Coupons (1100 °C, 2 h, N_2) with and without Polarization Testing 44
A.24. Comparison of the Chromium Peaks on the "As Nitrided" Case (After Sputter) with the Characteristic Cr Metal Peak..... 44
A.25. Schematic Representation of the Cross Sectional Areas of the Ni-50Cr Nitrided Coupons (1100 °C, 2 h, N_2)..... 45

CHAPTER 1
INTRODUCTION

The interest in developing more efficient and clean power sources has increased over the last decade. Fuel cells represent a promising answer for this problem by offering near-zero emission power generation at high efficiencies. However, this technology has not been entirely developed and there are still several important issues that have to be resolved in order to obtain maximum benefits from these devices[1,2]. Some of these problems are related to the materials selection and the cost involved for future commercialization[1]. In the specific case of polymer electrolyte membrane (PEM) fuel cells, the acidic environment generated at the polymer membrane, in addition to the necessity for full hydration, generates a very aggressive environment for all the components. Moreover, this membrane is also very sensitive to any contamination[2], especially metallic ions, which limits the choices available for component manufacture.

Bipolar plates are the components in the PEM fuel cells responsible for electrical contact among the various cells, and, at the same time, their surfaces provide patterns that guide the reaction gases and reaction products as they enter and leave the cells. For materials selection purposes, some of the characteristics that have to be taken into consideration are the electrical conductivity, thermal conductivity, chemical compatibility, corrosion resistance, mechanical strength, gas tightness, weight, volume and manufacturability[2].

Graphite is the most commonly used material for bipolar plates. However, it has some disadvantages, such as low mechanical strength, high porosity, low conductivity and high fabrication costs[1]. As a consequence, thick plates have to be used and a low volumetric power density problem is present. Therefore, carbon-carbon composites, carbon-polymer composites and metals are being studied as possible materials[1,2,3].

Although carbon-carbon composites and carbon-polymer composites have shown promising results[4], there are still some issues related to the overall power densities that can be achieved by these systems, as well as, their manufacturability in large scale[1]. On the other hand, metals offer higher electrical and thermal conductivities and better mechanical properties than graphite. As a consequence, research has been focused on low cost, high corrosion resistant and easy to shape alloys. Stainless steels are attractive from a cost and manufacturing standpoint; however, most have exhibited inadequate corrosion resistance in the PEM fuel cell environment. Several authors have reported decreases in the process efficiency due to the formation of resistive surface oxide layers on the plates and metal-ion contamination on the polymeric membrane[5,6].

The use of protective coatings can help overcome this problem. Metal nitrides have been identified as promising coatings due to their high electrical conductivity and good corrosion properties[2]. However, many conventional deposition methods typically leave through thickness pin-hole defects [7, 8]. Thermal nitridation has been proposed as an approach to form pin-hole defect free coatings[9]. One of the advantages of this nitridation

technique comes with the fact that the high temperatures enhance the reaction kinetics and the diffusion processes between the gas and the metal interface. As a consequence, all the reacting metal at the surface can be expected to form nitrides and pin-hole through thickness defects typically observed by conventional deposited coating techniques are not expected to form.

Proof of principle for thermal nitridation as a protection approach for metallic bipolar plates was reported by Brady et al[9]. The corrosion resistance of nitrided Tribocor 532N[10], Nb-30Ti-20W (wt%), was tested by the immersion of samples in aerated sulfuric acid solutions at pH 2 and pH 6 held at 80 °C for a period of 300 h. In addition, a Nafion polymer membrane was also placed alongside inside the solution. The weight loss reported was negligible, and the analysis of the membrane revealed that the contamination level was less than 1% of the active area. The long term contact resistance in a simulated bipolar plate environment was also tested, obtaining very good results in comparison with 316SS and aluminum. However, the substrate niobium-based Tribocor alloy is also resistant to corrosion in sulfuric acid; consequently, the results obtained did not fully establish that the nitrided surface was defect free. Even though this alloy represents a very good option for bipolar plates, it is too costly for most commercial fuel cell applications.

Recent work has shown that thermally grown Cr-nitrides on Ni-Cr base alloys show promise as a means to protect metallic bipolar plates for use in PEM fuel cells[9]. Depending on the nitridation conditions, CrN (cubic), Cr_2N (hexagonal), and $Cr_{10}Ni_7N_3$ (known as π phase[11]) phases can be formed. This study was focused on developing a better understanding of the corrosion properties of the nitrides present on the nickel-chromium system as a function of the nitriding temperature and time in pure nitrogen environments.

CHAPTER 2
IMPORTANCE OF THIS RESEARCH

Fuel cells are devices that produce electrical energy from the chemical energy of a fuel[12], usually hydrogen. As mentioned before, this technology is not completely developed and improvement of the materials currently used for manufacturing its different components will lead to a more efficient process and easier commercialization. For practical purposes the key target on the design of bipolar plates is to get the best performance in a compact and light weight PEM fuel cell stack[13]. The use of metallic bipolar plates with surface treatments as protective coatings against corrosion offers a potential solution to overcome the existing disadvantages of machined graphite. Nevertheless, a better understanding of the corrosion behavior of these nitrides correlated with its corresponding microstructure is still needed in order to design a specific nitrided procedure that will allow maximizing its properties under the PEM fuel cell acidic environment.

CHAPTER 3
REVIEW OF RELATED LITERATURE

3.1. Fuel Cells. General Concepts. Different Types of Fuel Cells.

Fuel cells can be defined as "electrochemical energy conversion devices"[12]. In other words, they convert the chemical energy of a fuel into electrical energy. This mechanism is two or three times more efficient than the one used in internal combustion engines for the generation of power[12].

The principle of operation is based on the electrochemical oxidation of a fuel and the reduction of an oxidant, as illustrated in figure A.1 and A.2 for a PEM fuel cell. In the PEM fuel cell the main process consists of two separates gas flows, one of hydrogen (fuel) and the other of oxygen (oxidant). Each gas flows along the channels of the surface of a plate (flow fields). These plates are separated by a membrane that has a catalyst-coated membrane. The catalyst will accelerate the separation rate of hydrogen and oxygen into their ions. The membrane will only permit the hydrogen ions to pass through, so electrons use the external circuit for moving from one side to the other, generating electricity. The hydrogen and oxygen ions will form water on the cathode, or oxygen, side. Heat will also be produced.

A single fuel cell typically operates in the range of 0.7V at 1 A/cm^2, one way to obtain useful levels of power is by connecting a number of cell together in a stack, so for two cells it will be 1.4 V (0.7x2), for three 2.1 V, etc[12]. A schematic diagram of three fuel cells scathed in series is shown in figure A.3. When a stack is made, the component that connects one fuel cell to another will have an anodic environment on one side and a cathodic environment on the other. This component known as a bipolar plate.

Even though fuel cells are often very sensitive to certain contaminants that may come from the fuel, as well as be produced internally, it is an attractive source of energy for an immense variety of applications such as: vehicular, stationary power, portable power, renewable energy[14], fast and easy start-up, among others. It has advantages over existing power generating devices, for example: high energy conversion efficiency, operation at constant temperature, near-zero emissions (unless it is operating with hydrocarbon fuels)[15], no moving parts (which will make the process more efficient and quiet), size flexibility, modular design, etc.

There are several types of fuel cells; each one is classified depending on the electrolyte used and the temperature of operation. The general properties of the fuel cell will depend on the physicochemical and thermomechanical characteristics of the materials used for each component: the electrodes, electrolyte, current collector, etc[16]. Because of the electrochemical nature of the process, determining the operating temperature of each type is very important. There are five main types of fuel cells: PEM Fuel Cells, Alkaline Fuel Cells (AFC), Phosphoric Acid Fuel Cell (PAFC), Molten Carbonate Fuel Cells (MCFC) and Solid Oxide Fuel Cells (SOFC). Some of the

differences and/or principal characteristics of the fuel cells are given in table A.1. This work focuses on PEM fuel cells.

3.1.1. Polymer Electrolyte Fuel Cells.

The main characteristic of this type of fuel cell is that the electrolyte used is a polymeric membrane that allows ion exchange from the anode to the cathode (proton conductor) inside each cell. This idea was first conceived by William T. Grubb in 1959[16].

As mentioned before, the only liquid handled in this type of fuel cell is the water obtained as a product of the reaction between oxygen and hydrogen. It is important to have a balance between the production and evaporation rates of water in order to keep the membrane hydrated, which is a critical factor for the performance of the cell. On the other hand, flooding can also take place causing diffusion problems from the gas to the electrode. As a consequence, the operation temperature for the existing low temperature PEM fuel cells is usually less than 120 °C[16]. However, some research has been focused on the development of membranes that allow higher operation temperatures when fuels other than hydrogen (e.g. methanol) are used[17,18].

The basic components of a polymer electrolyte membrane fuel cell are the proton conductor membrane (usually made of perfluorosulphonic acid polymer[16]) packed inside two porous electrodes impregnated with a catalyst (Pt), and the bipolar plates. The operating conditions of a low temperature PEM fuel cell are shown in table A.2.

3.1.1.1. The Polymer Membrane.

The polymer membrane functions as the electrolyte inside the cell. When the polymer membrane technology was being developed, strong acids were used for improving the contact between the electrodes and the membrane, even though further experiments showed that it was not necessary[16]. So, the only electrolyte needed for its proper working is the membrane.

The thickness of the membrane varies from 50 to 175 microns[12]. One of the most common materials for this application is Nafion® (perfluorosulfonic acid/PTFE copolymer in an acid form[19]). Because these membranes are based on a Teflon® backbone, they are very stable and comparatively rigid compounds.

It is very important for the Nafion® membrane to be fully hydrated. When the contact surface between the membrane and the electrode dries out, approximately above 90 °C, there is an increase in the resistance of the electrodes, and the oxygen reduction rate falls, decreasing the efficiency of the process.[20]

The key point of this type of membrane is that in the presence of water, only the hydrogen ions (or protons) are able to move freely through it, allowing the positive charges to go from one side of the cell to the other, while keeping the gases safely separated.

3.1.1.2. The Catalyst.

The oxygen reduction rate is almost 100 times slower than the hydrogen oxidation rate; this generates the necessity of using a catalyst[12].

Even though it is rare and costly, platinum (Pt) is the catalyst used for this type of application. Its importance lies in its very good performance under low temperatures, such as 80 °C[12,16,19].

A thin film of the catalyst is spread over the surface of the electrodes. The amount of platinum used varies depending on the manufacturer, but currently it is about 0.5 mg/cm^2 of membrane, a small number in comparison with the original 4 mg/cm^2 when it was first made in the 1960s by the people of the Gemini space program[12].

One of the major disadvantages of this catalyst is that its tolerance of CO at 80 °C is very low, only a few ppm[16]. Another problem is that only the platinum on the surface will help the reactions to occur[12], so the platinum beneath that plane is only increasing the costs of production.

3.1.1.3. The Electrodes.

An electrode can be defined as "a conductor used to establish contact with an electrolyte and through which current is transferred to or from an electrolyte"[21].

The electrochemical reactions will take place at the electrodes, so, a three phase interface is established among the electrodes, the membrane and the reactants. The behavior of this interface will have a very important role in the electrochemical performance of the cell. In the fuel cell technology, the plates that sandwich the membrane are the electrodes.

There are two electrochemical reactions taking place at the plates of a PEM fuel cell. One is the oxidation half reaction on the hydrogen side, and the other is the reduction half reaction on the oxygen side. The total products of the reaction are heat, water and electric power. These reactions are the following[12]:

Oxidation Half Reaction: $2H_2 \rightarrow 4H^+ + 4e^-$

Reduction Half Reaction: $O_2 + 4H^+ + 4e^- \rightarrow 2H_2O$

Cell Reaction: $\mathbf{2H_2 + O_2 \rightarrow 2H_2O}$

3.1.1.4. The Bipolar Plates.

As mentioned before, the functions of bipolar plates are to deliver fuel gas and oxygen to the membrane, carry out the reaction products and make the electrical contact of the cell in series.

According to Borup et al.[2], for high efficiency performance the voltage loss must be less that 10 mV/plate for an operating current of 1 A/cm^2. Plate resistance must be less than 0.01 Ωcm^2 per plate. In the presence of metals with coatings about 25 μm thick, the coating resistivity must be less than 4 Ωcm. Corrosion processes inside the cell can also induce the formation of resistive surface layers, increasing the resistivity.

Several materials have been tested for possible bipolar plate application, e.g. stainless steals[6,22]. Moreover, there are other studies involving pure metals, such as pure titanium[23] and aluminium[23,24], both of which behave very poorly in the PEM fuel cell environment, the former by presenting high surface resistances and the latter by corroding very fast.

Even though it implies a significant increment in the production cost, the use of low surface resistance coatings, such as metal nitrides, carbides and some oxides, has been applied to several metals and alloys as a solution to this problem. Gold[23], TiN[7,9,23] and chromium nitrides[9] have been studied. Hentall et al. reported the use of gold plated on aluminum[22]. The system proved to be very reactive and contamination of the membrane occurred very fast due to the lifting of the gold coatings. Uchida et al. studied TiN coatings on 316SS substrates[7]. A significant amount of pin-hole defects were observed after nitridation. These defects tended to decrease with thicker TiN layers. However, after a certain thickness the occurrence of cracking and peeling of the coating was observed additionally to the pin-holes present. As a consequence, the dissolution of the substrate was likely to occur over long term tests.

3.2. Electrochemical Corrosion.

Corrosion can be defined as "the deterioration of materials due to reactions with their environments"[25]. The deterioration mechanism is an atomic, molecular, or ionic transport process that occurs at the interface of the material and environment. Electrochemical corrosion involves the generation of ions and the movement of electrons in order to maintain a charge balance in the system.

In the simplest case of corrosion in aqueous environments, a thermodynamically unstable solid metal (M) will try to form its ion (M^{m+}) so it can move into the solution, or electrolyte. In this process electrons are being generated ($M \rightarrow M^{m+} + me^-$); so, the metal is oxidized and a loss of material is occurring. The electrode at which this reaction (chemical oxidation) takes place is known as the anode. After the metal ions are released they will do one of the following: form complex ions or combine with other species

present in the solution to form oxides, hydroxides or sulfides[25]. The anodic reaction is sustained by the consumption of electrons by a cathodic reaction ($X^{m+} + me^- \rightarrow X$). Similarly to the anode, the electrode where this reaction (chemical reduction) takes place is known as the cathode.

The potential difference between the anode and the cathode in the cell is the driving force for the corrosion reaction, and the corrosion rate will be directly proportional to the current that flows through the cell[25].

One way of measuring the corrosion behavior of a material is by using what are called polarization curves. Figure A.4 represents the anodic polarization curve of an active-passive material. These types of plots help to establish the relationship between the measured potentials (E, V or mV) relative to a reference electrode and their respective currents (I, A) or current densities (i, A/cm^2). Three major regions can be identified from this figure: the active, passive and transpassive regions.

Usually, polarization scans start below what is known as the corrosion potential (E_{corr}), which represents the potential value at which the currents (or current densities) for the anodic and cathodic reactions taking place at the same time are equal. In other words, at E_{corr} the current density can be represented as $i_{corr}=i_a=i_c$, where i_a and i_c are the anodic and cathodic current densities, respectively, and i_{corr} is the corrosion current density.

In the active region the oxidation reaction is taking place and the material is corroding. As the potential increases, a critical value is reached, known as the passivation potential (E_{pp}), and the current density decreases drastically. This behavior is associated with the formation of a protective phase (usually an oxide) over the surface of the material that is exposed to the electrolyte. The degree of protection that this phase can offer will vary depending on its porosity and adhesiveness. The maximum value of the current density is known as the active peak or critical anodic current density (i_{crit}) and the new and lower value is called the passivation current density (i_p). The region at which the material is self protected against high current densities is known as the passivation region.

As the potential keeps increasing, the current density may start increasing again. The potential at which this occurs is known as the breakdown potential (E_b). This behavior is related to dissolution of the protective film, either uniform dissolution (transpassive behavior) or localized dissolution (pitting or crevice corrosion).

The value of the corrosion current density, i_{corr}, becomes very important in determining the corrosion rate of a material under open-circuit conditions (E_{corr}). From Faradays's law it can be shown that the corrosion current density value is directly proportional to the corrosion rate.

Temperature has an important effect on the corrosion rates. Usually, the rate at which any metal corrodes is directly proportional to the temperature. This is due to the

increase in thermal energy available for the activation of chemical and electrochemical reactions and the increase in the diffusion rates in the electrolyte[21]. However, this relationship between temperature and corrosion rate is not always true. The change in this pattern is related to the stability of the passive film at the surface of the material, which behavior can be drastically affected depending on the overall set of environmental conditions. The temperature of the sample itself is also a very important factor. In most of the cases, the corrosion rate of the heating elements in a device (such as heat exchangers) is higher than that of the rest of the equipment.

3.3. Nickel and Nickel – Chromium Alloys.

This effort is focused on thermal nitridation of Ni-Cr alloys for bipolar plate applications. Nickel is well known for its high corrosion resistance in reducing environments, as well as the formation of a passive, corrosion-resistant oxide film under oxidizing conditions. On the other hand, chromium is well known for its ability to increase corrosion resistance at lower temperatures, and also for improving the resistance of nickel to oxidizing acids. By reducing the protection potential (E_{pp}) and the critical anodic current density (i_{crit}), this element enhances the passivation of nickel[25]; so the more chromium present in the alloy, the easier it becomes passivated. There are other alloy elements quite significant in the enhancement of corrosion resistance, such as copper, molybdenum, and tungsten.

In general terms, nickel-base alloys are known for being very effective corrosion-resistant materials in extreme temperature environments, and very resistant to severe operating conditions (involving liquid or gaseous environments, high stresses, and combinations of these factors). However, the electrical resistivity of the alloy tends to increase directly proportional to the amount of chromium present in the system. In addition, the brittleness of the α-chromium phase produces an increase on the strength and a decrease in the ductility with increasing of chromium content in the alloy[26].

The phase diagram of the Ni-Cr system is shown in figure A.5; nickel has a face center cubic (fcc) crystal structure, and chromium a body centered cubic (bcc). Ni-Cr alloys will have an fcc structure from 0 to about 40 wt% Cr. From approximately 40 to 90 wt% Cr, it will have a two-phase crystal structure, and from 90 to 100 wt% Cr it will have a bcc structure[25].

3.4. Oxidation of Metals.

In the presence of gaseous oxygen almost all metals are thermodynamically unstable, resulting in the formation of an oxide, which "frequently constitute protective layers that separates the metal from the gaseous oxygen, thereby inhibiting further oxide formation"[28]. Oxides are only one of several types of protecting layers on metals. Depending on the ambient gas, the metal composition and the reaction conditions,

sulfides, chlorides, carbides, nitrides, etc. can also be formed[27]. In the general case, the word oxidation refers to the increase in valence state (loss of electrons) in a specie that is undergoing a chemical reaction; thus, the term "oxide" can be extended to any type of these protective layers.[29,30]

The adhesion of the oxide film to the metal surface is a very important factor. Generally, when scaling resistance is not high enough, spalling of the scale may happen and the life time of the material will be considerably reduced as a result of the rapid oxidation (reduction of the cross section), bringing as a consequence the necessity of a premature replacement. In addition, the oxidation products can affect the efficiency of the system in which they are interacting.

At high temperatures, when the oxide film is being formed, it often develops as a compact phase over the reacting surface of the metal. For oxidation to keep occurring, at least one of the reactants has to diffuse through the film in order to find its reaction partner. As described by Hauffe[30], some of these processes are the following:

1. "Phase-boundary reactions (chemisorption of the nonmetal molecules with simultaneous electron exchange and splitting of the molecules at the gas/oxide interface and transfer of the metal from the metallic phase, in the form of ions, and electrons, to the scale at the metal/oxide interface with further reaction of the individual reactants and formation of the reaction product), nucleation, and crystal growth.
2. Diffusion or transport of cations, anions, and electrons through the scale, complicated by the special migration mechanism because of the appearance of chemical and electrical potential gradients in the scaling or tarnishing layers.
3. Predominant transport processes in space-charged boundary layers in the case of thin tarnishing layers, especially at low temperatures.

Two further factors are also significant for the formation, composition and structure of the scaling layer:

4. The thermodynamic stability of the oxide that is formed.
5. The crystal structures of the scaling layer and of the metal or alloy, which determine the adhesion between the scaling layer and the underlying metal".

Assuming that the diffusion rate will determine the velocity of the process, the generation of an oxide film can occur in two ways: internally or externally. The internal oxidation is the process by which oxygen (or any oxidant gas) diffuses into an alloy and causes sub-surface precipitation of the oxides (or the species produced depending on the gas) of one or more alloying elements[28].

According to Birks and Meier[28] there are four necessary conditions for the internal oxidation process to take place:

1. "The Gibbs free energy of formation per mol O_2, ΔG^{θ}, of the solute metal oxide, BO_v, must be more negative than that of the base metal oxide.

2. ΔG for the reaction $B + \nu O = BO_\nu$ must be negative. Therefore, the base metal must have a solubility and diffusivity for oxygen that is sufficient to establish the required activity of the dissolved oxygen at the reaction.
3. The solute concentration of the alloy must be lower than that required for the transition from internal to external oxidation.
4. No surface layer must prevent the dissolution of oxygen into the alloy at the start of oxidation."

The internal oxidation process in a metal implies inward diffusion of the oxygen dissolved in the base metal. This dissolution can occur at the surface of the specimen, as well as at the metal-scale interface (in the case of the presence of an external scale). The inward diffusion of the reactant gas and the outward diffusion of the solute (oxidizing metal) at the reaction front determine the critical solubility product for the nucleation of precipitates. Variations in the solute concentration will occur, and nucleation and grow will take place until the reaction front reaches a solute depleted area.

When the initial solute concentration increases and the solubility of the oxidant gas decreases, the penetration velocity of the oxide also decreases, as establish by the following equation for an AB alloy:

$$v = \frac{dX}{dt} = \frac{N_O^{(S)} D_O}{\nu N_B^{(O)}} \frac{1}{X}$$

where $N_O^{(S)}$ is the solubility of the oxidant gas in A, D_O is the diffusivity of the oxidant gas in A, and $N_B^{(O)}$ is the initial solute concentration[26]. This implies that for a given oxidant gas and solute under a certain set of conditions, there is a limiting value on the concentration of solute above which its diffusion rate can be high enough to form a precipitation product able to block the oxidant gas to get into the metal stopping the internal oxidation (nitridation)[27,28,29]. The reaction front will move outwards (and parallel) to the surface. In the presence of an alloy, this process can be used for the selective oxidation of a solute (Cr, Al, Si, etc.) in order to protect the parent metal (Fe, Ni, etc.). These fundamental principles also apply to other reactive gaseous species, such as nitrogen.

3.5. Nitridation of Nickel-Chromium Alloys.

Depending on the conditions at which the nitridation process is developed, basically two morphologies can be obtained: CrN (cubic) or Cr_2N (hexagonal). In Ni-Cr systems $Cr_{10}Ni_7N_3$ also can be found. This is known as the π phase and is formed from the peritectiod reaction between Cr_2N and pure nickel from the matrix[17,31,32].

R. P. Ruby et al. examined the internal nitridation of Ni-Cr alloys in NH_3 environments at 700, 800 and 900 °C for chromium compositions from 10 to 50 wt%[33]. X-Ray Diffraction (XRD) scans showed only the presence of cubic CrN in all samples. It

was also observed that the transition from internal to external nitridation occurred between 30 and 40 Cr wt% at 900 °C. A. Kodentsov et al. studied the nitridation process in Ni-Cr alloys at 1125 °C in a pure nitrogen atmosphere[32]. The chromium concentration of the samples was varied from 5.19 to 33.19 wt%, and the nitrogen pressure, from 0.986 to 5922 atm. For a pressure range 98.7 to 5922 atm of N_2 and a chromium atomic concentration equal or higher than 29.04 %, the transition from CrN to hexagonal Cr_2N was observed. The formation of the π phase was observed at 1000 °C and became unstable at 1100 °C.

U. Krupp and H. J Christ studied the internal nitridation of nickel-based alloys in a nitrogen atmosphere[31]. At 900 °C, for the Ni-10Cr (wt%) coupons no nitride was found. However, at the same temperature for chromium concentrations of 20 wt% and higher, internal CrN precipitation was detected. Around 30 Cr wt%, Cr_2N and the ternary phase π were observed mostly at the grain boundaries, but were also found at the surface. U. Krupp et al. also investigated the occurrence of the ternary π phase during nitridation of nickel-chromium alloys[11]. In this case, alloys with 10, 20 and 30 chromium weight percent were nitrided in a temperature range from 800 to 1100 °C for different time intervals. All the samples underwent nitridation, although for chromium concentrations below 30 wt% only cubic CrN was present. At 30 wt% the coating present was a mixture of Cr_2N with ternary π phase at the grain boundaries. For temperatures higher than 1000 °C the ternary phase became unstable and it was only found immediately below the surface.

K. Tjokro and D. J. Young studied the internal nitridation behavior of stainless steels (mainly Fe, Ni and Cr) at 1000 and 1100 °C in a nitrogen environment[4]. For both temperatures Cr_2N was found as an external non-uniform, Cr_2N scale and as the only chromium precipitated internally in the samples. In the case of CrN, it was only found at the surface when the temperature was 1000 °C.

The gas nitridation of pure chromium as a function of time was studied by Buijnsters et al[34]. The selected temperature was 800 °C and the times varied from 1 to 142 h. For all the initial times it was found that the CrN and Cr_2N phases were forming at the surface. However, the CrN fraction at the surface increased with time until the Cr_2N disappeared completely from the surface. It is suggested that above 800 °C the CrN can be formed by the reaction of the Cr_2N with nitrogen ($2Cr_2N_{(s)} + N_{2(g)} \rightarrow 4CrN_{(s)}$), which will explain the Cr – Cr_2N – CrN layer sequence also reported by other several authors.

Zenguh H. et al. studied the influence of the nitrogen partial pressure on the microstructure, phases and composition of CrN_x films obtained after using the magnetron sputter technique[35]. The films were deposited in an argon-nitrogen mixture atmosphere. The nitrogen partial pressure varied from 0.005 to 0.3 Pa, and the argon partial pressure was kept at 0.3 Pa in all the cases. The substrate used was high purity chromium. A single CrN phase was not observed in any of the cases. However, the nitrided films varied from Cr+Cr_2N to a single Cr_2N phase; and then from a CrN+Cr_2N to a nearly single CrN. It

was observed that the relative amounts of nitrogen on the CrN_x films obtained had the tendency to increase as the nitrogen partial pressure increased.

Similar results were presented by Zhou Q. et al in the study of corrosion resistance of duplex and gradient CrN_x coated steels where the N/Cr ratio increased with the nitrogen partial pressure[36]. The main composition of the coatings obtained varied from Cr, Cr_2N to CrN; and even though a stoichiometric CrN composition was not reached it was more likely to be found at higher nitrogen partial pressures.

3.6. Corrosion Behavior of Chromium Nitrides.

M. Taguchi et al. studied the effect of surface nitriding on the corrosion resistance of pure chromium[37]. The nitridation was made in a pure nitrogen atmosphere at temperatures from 500 to 1200 °C. At 600 °C a mixture of α-Cr and Cr_2N was found on the surface; no nitrides were found below this temperature. From 700 to 1000 °C a combination of CrN and Cr_2N was observed. Above 1100 °C the CrN became unstable and a single Cr_2N phase was formed. For the corrosion resistance measurements, anodic polarization curves (from -0.8 to 1.2 V(Ag/AgCl)) and immersion tests were performed both in a 1 $kmol \cdot m^3$ of sulfuric acid solution at 40 and 100 °C respectively. Cubic CrN was found to have better corrosion resistance properties. Any of the samples treated below 600 °C developed passive films under the polarization test; although, above 700 °C the corrosion potential was very similar among the samples, around -0.43V (Ag/AgCl), and active dissolution did not occur. During the immersion test all the specimens nitrided below 700 °C (mixture of α-Cr and Cr_2N) dissolved. The amount of chromium dissolved into the solution decreased with the nitriding temperature until it became very small at 1000 °C (CrN + Cr_2N). The single Cr_2N phase was rapidly attacked. However, there is no specific information on the continuity or thickness of the nitride layers formed on the surface.

M. Taguchi et al. also studied the corrosion behavior of chromium nitrides obtained by reactive ion plating on glass substrates[38]. Three different surface products were obtained: Cr and N(α-Cr) solid solution, mixture of Cr_2N and CrN, and a single CrN phase. The best corrosion resistance in 1 $kmol \cdot m^{-3}$ H_2SO_4 at 100 °C was observed for pure CrN phase. The Cr and N(α-Cr) layer corroded very fast, although the Cr_2N of the CrN+Cr_2N mixture was selectively attacked.

G. Bertrand et al. studied the corrosion behavior and protective quality of chromium nitride coatings obtained by sputter deposition over different substrates[39]. The coatings studied were CrN and Cr_2N, which at the same time were compared with pure chromium. High concentrations of surface defects were observed in both coatings; moreover, they were more frequent on the Cr_2N coat. For corrosion resistance tests, two electrolytes were used, aerated 0.5 M H_2SO_4 and 3% NaCl solutions at room temperature. The polarization curves showed that CrN had lower I_{corr} and higher E_{corr} in acidic

conditions, which indicated better corrosion resistance; although the corrosion behavior was directly affected by the number of defects present on the coating surface.

M.P. Brady et al. studied the corrosion protection of nickel-based alloys by thermal nitridation[9]. In the case of nickel-chromium alloys, the heat treatment was made in a nitrogen atmosphere at 1100 °C for one or two hours. Despite the chromium concentration of the sample; 35, 45 or 50 wt%, the microstructure obtained in all the cases included a mixture of chromium depleted Ni(Cr) and ternary π phase, directly below Cr_2N at the surface. The continuity of the Cr_2N layer improved directly with increasing chromium concentration; hence, the overall corrosion resistance of the system also improved. Even though there is no reference about the presence of CrN on the coupons, it mentions the CrN as a potential protective coating for bipolar plates in PEM fuel cells.

CHAPTER 4
EXPERIMENTAL METHODS

4.1. Sample Fabrication and Preparation.

A series of model Ni-X (X=Cr, Nb, Ti,V) alloys were prepared by arc melting and drop casting in a chilled copper mold. The castings were typically vacuum heat treated at 1100° C for 8 h. Coupons of 1-1.5 mm thickness were cut with an electrical discharge machine (EDM) from the castings and prepared to a 240 grit finish using SiC paper. Each sample was weighed after finishing the surface preparation.

4.2. Heat Treatment.

Nitridation was conducted in an alumina vacuum furnace backfilled with high-purity nitrogen to 1 atmosphere. The nitrogen flow was stopped, and then the coupons were heated to 875-1100 °C for times ranging from 1-30 hours. Nitrogen was not continuously flowed during the nitridation run to prevent the constant introduction of trace oxygen impurities present in the nitrogen into the system. An additional Ni-50Cr coupon was also nitrided in 90%Ar-10%N_2, following the same procedure as with the pure nitrogen. Each sample was weighted after nitridation in order to measure the amount of nitrogen gained by the sample, normalized by the surface area of the coupon.

4.3. Sample Characterization.

Characterization of the nitrided samples was performed before and after the corrosion testing by scanning electron microscopy (SEM) and electron probe microanalysis (EPMA) (both surface and cross-section), as well as by X-Ray diffraction using Cu K-α radiation. X-Ray Photoelectron Spectroscopy (XPS) analysis was also used on select samples to establish the differences on the surfaces before and after polarization in order to determine the nature of the corrosion products.

4.4. Corrosion Behavior.

Corrosion behavior of the nitrided samples was evaluated by anodic polarization testing. The scan rate was of 0.1 mV/s, a saturated calomel electrode (SCE) was used as reference electrode and the electrolyte employed was sulfuric acid (H_2SO_4) at a pH of 3 and a temperature of 80 °C. Aerated conditions were used to simulate bipolar plate cathode environment conditions. Select samples were also analyzed under simulated bipolar plate anode environment conditions by purging the electrolyte with a gas mixture consisting of Ar-4%H_2.

The electrical contact between the coupon and the potentiostat was achieved with the attaching of the sample (by spot welding) to a specimen holder (which manly consisted on a titanium wire). In order to control the area of the specimen exposed to the electrolyte, the unwanted parts of the surface were covered with two coats of an insulating enamel resistive to the aggressive electrolyte (Glyptal®). The idea was to leave unprotected a nice flat surface.

Before starting any polarization scan, the solution was heated up to 80 °C and the corrosion sample was placed in the electrolyte when this temperature was reached. In the case of the aerated environment, a constant flow of air was sparged into the electrolyte. The sparge started as soon as the sample was placed in the solution. Before starting any screening, the potential measured by the potentiostat was allowed to become stable in order to obtain the corrosion potential (E_{corr}). The corrosion tests were started 50 mV below the open-circuit corrosion potential and were ended at 1000 mV (SHE). For the deaerated environment simulation the same procedure was followed, the only difference was the sparging of Ar-4H_2 instead of air in the electrolyte.

An additional screening of the change in current density against time (at a fixed potential) was performed immediately after the polarization test for some of the samples. The potential was held at 1000 mV(SHE) or 750 mV(SHE) for a 5 hour period without changing the electrolyte.

CHAPTER 5
RESULTS AND DISCUSSION

5.1. Polarization Tests.

5.1.1. First Approach.

In order to obtain an approach for possible high corrosion resistance alloys for fuel cell applications, polarization screening was performed on several different types of alloys with different heat treatments. All nitrides were obtained in a pure nitrogen atmosphere. Figure A.6 shows selected results from the tested model nitrided alloy groups. The only systems that gave low corrosion currents were the nitrided Ni-Ti and Ni-Cr model alloys, which for potentials of ~800 and ~900 mV(SHE), respectively, offered current densities on the order of $1x10^{-6}$ A/cm^2. In the case of the nitrided Ni-Ti alloy, little increase in corrosion current was observed between 800 and 1000 mV(SHE), while the nitrided Ni-Cr sample showed a rapid increase in corrosion current above 900 - 950 mV(SHE). However, the TiN surface formed on the Ni-Ti alloy showed evidence of local attack and surface cracking after testing. No attack was evident on the nitrided Ni-Cr alloy coupon after corrosion testing. Therefore, the nitrided Ni-Cr system was selected for further study.

5.1.2. Nitrided Nickel - Chromium Alloys.

Temperature/time of nitridation had a noticeable effect on the corrosion behavior. Figure A.7 shows the anodic polarization behavior of the coupons in aerated sulfuric acid electrolyte at pH 3 and 80 °C. In all cases, nitridation proved to be effective for improving the corrosion protection in comparison with the uncoated Ni-50Cr alloy. In fact, corrosion resistance tended to increase with the increase of nitriding temperature.

The open-circuit corrosion potential was lower for the uncoated case, around 150 mV(SHE). This sample also presented active dissolution until it reached the passivation potential at ~445 mV(SHE) and a current density of $1x10^{-6}$ A/cm^2. The passivation regime started breaking close to 700 mV(SHE), where it became rapidly active again.

The corrosion potentials for the nitrided coupons fell in a range from 340 to 550 mV(SHE), and tended to increase with the temperature of nitridation. The current densities observed were somewhat low even at high potentials. However, there were small current densities that can be associated with the formation of corrosion products. Similar, for all the different nitrides, when a certain potential was reached the current densities started to increase rapidly. The best corrosion resistance was given by the nitridation case of 1100 °C and 2 h, where for potentials as high as 900 mV(SHE) current densities on the order of $1x10^{-6}$ A/cm^2 or less were obtained. There was no indication of pitting corrosion on any of the coated samples after the polarization tests.

As an attempt for decreasing costs and ease of production, the reduction of chromium in the alloy was a tentative target. Nevertheless, figure A.8 shows that the protective layer obtained on the surface was dramatically affected by the amount of chromium in the alloy. The behaviors of both Ni-35Cr and Ni-45Cr were very similar and the gained weight during nitridation for 2 h at 1100° C in pure nitrogen was 0.98 and 1.87 mg/cm^2 respectively. However, the current densities were significantly higher than those obtained for the Ni-50Cr coupon, which had a weight increase on the order of 1.9-2.3 mg/cm^2 under similar nitridation conditions. The level of corrosion protection under this environment is associated with the different microstructrures/morphologies of nitride obtained; however, this effect will be discussed in the next section. It will be necessary to modify the nitridation treatment used for the Ni-35Cr and Ni-45Cr (different temperatures, times, nitridation environments), likely in combination with alloying additions, in order to get alloys in this Cr range to form a similar corrosion resistant Cr-nitride surface as that exhibited by the nitrided Ni-50Cr.

The effect of the nitrogen partial pressure (activity) on the nitriding behavior is shown in figure A.9 for Ni-50Cr. The weight gained by the coupons under the pure nitrogen and the Ar-10%N_2 atmospheres for 2 h at 1100° C were 2.37 mg/cm^2 and 1.47 mg/cm^2 respectively. As can be seen, under the same heat treatment the protective coating obtained with pure nitrogen was remarkably better for corrosion protection than that obtained with the mixture of Ar-10%N_2, which has a very similar behavior to the uncoated alloy. Similarly, the nitride microstructure and morphology issues related to this tendency will be discussed further below.

5.1.3. Pure Chromium.

The effectiveness of the nitride coatings for corrosion protection on pure chromium in a sulfuric acid solution pH 3 at 80 °C is shown in figure A.10. The metallic chromium (uncoated coupon) exhibited fairly low corrosion rates as expected. In fact, for potentials from ~460 to 830 mV(SHE) the current densities increased slower than in the rest of the potentials scanned. Depending on the nitridation conditions, the corrosion rates became even lower. In the case of nitriding in Ar-10%N_2 atmosphere at 1100 °C for 2 h, the corrosion resistance was considerably higher than for the uncoated condition. The highest protection against corrosion was obtained in a pure nitrogen atmosphere, where for potentials varying from ~400 to 600 mV(SHE) the current densities decreased approximately an order of magnitude. However, the current densities obtained in all the cases for higher potentials were moderately higher than the goal of $1x10^{-6}A/cm^2$ or less. This effect is produced by the different phases obtained after nitridation which will be discussed later.

Consistently for all the coatings obtained in both pure nitrogen and Ar-N_2, the corrosion potentials seem to increase with the increasing nitrogen partial pressure.

5.2. Protective Quality.

Figure A.11 and A.12 show the variations of the current densities with respect to time in H_2SO_4 pH 3 at 80 °C as the electrolyte. These tests were performed immediately after the regular polarization tests. The level of protection given by the nitrides obtained will depend on the conditions at which they were exposed. Figure A.11 shows the behavior of the Ni-35Cr and 45Cr when the potential was held at 1000 mV(SHE) for a period of 5 hours. As can be seen during this time the current density increases almost one order of magnitude, reaching values even higher than $1x10^{-5}$ A/cm^2. In the case of figure A.12, when the potential was held at 750 mV(SHE), the protective layer just allowed current densities on the order of $1x10^{-6}$ A/cm^2 or less. The current densities observed for the Ni-35Cr coupon were higher than those of the Ni-50Cr. In fact, the currents densities for the Ni-50Cr were very stable and on the order of $2.5x10^{-7}$ A/cm^2, which is very close to the value obtained for this potential on the polarization scan shown in figure A.7.

5.3. Deaerated Electrolyte.

Figure A.13 shows the polarization curves obtained when the electrolyte (sulfuric acid pH 3 at 80 °C) was sparged with a gas solution of 96Ar-4H_2 in order to simulate bipolar plate anodic conditions. Ni-50Cr was evaluated for two nitridation conditions: 1100 °C for 2 h in pure nitrogen and 1100 °C for 5 h in Ar-10%N_2 (times adjusted to achieve similar nitrogen uptakes on the order of 1.9 - 2.3 mg/cm^2).

The run surveyed from –500 mV(SHE) to 500 mV(SHE). This allowed observing the effect of those highly negative potentials over the nitrided surface even though it was not possible to monitor the anodic polarization behavior until the E_{corr} value was reached. Moreover, the anodes of the PEM fuel cells typically operate in a range of -200 to 100 mV(SHE), which implies that this is the most important range of the curve.

In the case of the coupon nitrided in pure nitrogen, the corrosion potential measured before the start of the polarization test went as low as 200 mV(SHE), ~350 mV below the corrosion potential obtained for the same coupon in the aerated case. On the Ar-10%N_2 coupon the corrosion potential measured before the start of the polarization test went down to 100 mV(SHE), just around 100 mV below its value in the aerated environment.

In both cases the anodic current densities obtained through the entire screening were lower than $1x10^{-6}$ A/cm^2. The coupon nitrided in pure nitrogen presented a non-uniform coloration after the polarization test. However, inspection of the surface using an optical microscope did not show evidence of corrosion attack.

5.4. Correlation with Nitride Microstructures.

The corrosion protection can be attributed to the different microstructures and phases obtained under different nitridation conditions. Figures A.14 and A.15 show the cross sectional microstructures of the Ni-35Cr and 45Cr nitrided in a pure nitrogen atmosphere for 2 h at 1100 °C. As can be seen in figure A.14 for the Ni-35Cr case, the microstructure mainly consisted of a thin discontinuous layer of Cr_2N layer, less than 1 μm thick, overlying a mixed region of internal π phase and Cr_2N precipitates in chromium depleted Ni(Cr) metal. The nitrided microstructure on the Ni-45Cr (Figure A.15) consisted of a thicker layer of Cr_2N (~2μm) than that observed on nitrided Ni-35Cr overlying a layer of continuous layer of π phase ~1.5μm thick. Underneath was a zone of internal π phase and Cr_2N precipitates in chromium depleted Ni(Cr) metal, again similar to that observed for nitrided Ni-35Cr. Qualitatively, the Cr_2N layer formed on Ni-45Cr appeared was more continuous than that formed on Ni-35Cr, however gaps in the Cr_2N were still evident.

Figure A.16 shows a backscatter SEM photograph of the cross section after the polarization of a Ni-50Cr coupon nitrided at 875 °C for 30 h, which was the less corrosion-resistant nitriding condition obtained for Ni-50Cr. The microsructure was reminiscent of that observed for 1100° C, 2 h nitrogen nitrided Ni-35Cr and Ni-45 Cr with a layer of Cr_2N overlying a π phase layer, and an internally nitrided zone primarily of π phase dispersed in Cr-depleted Ni(Cr) metal. At the surface, the Cr_2N was not fully continuous; rather it was intermixed with π phase. The π phase sublayer was also much thicker than that observed on the 1100° C nitrided Ni-35Cr and Ni-45Cr, consistent with its greater stability at temperatures less than 1100° C.

Figure A.17 shows a typically cross section microstructure for Ni-50Cr nitrided at 1100 °C for 1-2 h in pure nitrogen, the condition that yielded the most corrosion-resistant nitrided surface. In this case, three phases were determined: a very thin and semicontinous CrN phase on the surface, Cr_2N in the middle and the π phase in between the Cr_2N and the chromium-depleted Ni(Cr)zone. In contrast with the nitrided microstructure formed on the 875 ° C, 30 h pure nitrogen nitrided Ni-50Cr (Figure A.16), and the 1100 ° C nitrided Ni-35Cr and Ni-45Cr (Figures A.14 and A.15), the Cr_2N phase formed on the 1100° C nitrided Ni-50Cr was continuous, more uniform, and considerably thicker (3-5 μm). The underlying π phase layer was also thinner than that formed at 875° C, 2 μm vs 9 μm- again consistent with the lack of stability of the phase above ~1100 °C. Although it was not definitively identified on all samples, it is likely that all the pure nitrogen nitrided Ni-Cr alloys examined contained at least trace quantities of the CrN phase at the surface.

Figure A.18 shows the cross sectional view obtained for the Ni-50Cr coupon nitrided in Ar-10%N_2 at 1100 °C for 2 h after polarization. This condition yielded the

lowest corrosion resistance of all nitridation conditions studied. The surface in contact with the electrolyte was a non-uniform Cr_2N over a fairly uniform π phase. Therefore, significant area fractions of both Cr_2N and π phase were present at the surface and exposed to the electrolyte. No CrN was detected, consistent with a reduced nitrogen activity in the Ar-10%N_2, compared to pure nitrogen, and the greater thermodynamic stability of Cr_2N.

Collectively, correlation of the nitrided microstructures with the corrosion behavior in aerated pH3 sulfuric acid at 80 °C indicate that the CrN+Cr_2N surface offers better corrosion protection under these conditions than does $Cr_2N+\pi$. The data also suggests that the π phase exhibits the poorest corrosion resistance of the nitride phases examined (CrN, Cr_2N, π). However, the inability to produce exclusive, single-phase layers of each nitride phase precludes a definitive conclusion, as the poor corrosion resistance may result from the phase mixtures rather than any inherent differences in corrosion resistance.

5.5. XPS Studies.

A key issue for PEM fuel cell applications is the mechanistic source of the corrosion currents obtained, even when the currents are of low magnitudes (10^{-6} A/cm^2 and less). If they result primarily from a dissolution process, this could result in membrane contamination and degradation of cell performance under long-term operation. A strong component of an oxidation/passivation mechanism to the corrosion current is preferred, as long as it does not result in a degradation of electrical properties (i.e. increased surface resistance), which also would degrade cell performance. In order to obtain a better understanding of the corrosion current source and probable corrosion mechanisms, X-Ray Photoelectron Spectroscopy (XPS) analyses were performed on the as-nitrided Ni-50Cr (1100 °C - 2h - N_2) surface and on a polarized Ni-50Cr surface (nitrided under the same conditions), which, after the regular polarization screening, was additionally held at 1000 mV(SHE) or 750 mV(SHE) for 5 hours.

A first XPS scan was performed over an energy range between 0 and 1200 eV on the as-nitrided surface. Results demonstrated the presence of carbon, oxygen, chromium, nitrogen, silicon and zinc (the last one less than 1 at%). No nickel was observed. A concentration profile with respect to the sputtering time of this surface is shown in Figure A.19. The principal assumption made was that the species following a similar trend were more likely to be working together. This tendency was observed in the case of the 'no-sputter' oxygen and carbon. No-sputter refers to the original surface before sputtering started. As sputtering began this carbon and oxygen were removed very fast suggesting that they may be related with adsorption products at the near surface.

As sputtering time increased, the atomic concentrations of a type of chromium, nitrogen and oxygen also increased in a similar manner until they reached a plateau;

referred to as 'sputter' species in figure A.19 since they appeared after sputtering started. These different forms of nitrogen and chromium can be associated with a chromium nitrided film. At the same time, the presence of oxygen suggests the existence of an oxidized layer as it gets closer to the nitrided film.

The evolution of these species as the survey went deeper into the surface can be appreciated in figure A.20, which shows the changes on the individual peaks of oxygen, nitrogen and chromium as the sputter time increased. In the case of oxygen, the type present right at the surface is different to one observed after sputtering for a short time, as indicated by the sudden change in the shape (width, height and peak position). This is related to a change in the oxidation state of the element. The nitrogen and chromium also evolved during the surveys; however, it was a more gradual transformation. The comparison between the chromium peak before and after sputtering will be discussed below.

In the case of the coupon held at 1000 mV(SHE) for 5 hours in the electrolyte, the first scan from 0 to 1200 eV showed the presence of carbon, oxygen, chromium and silicon. No nickel was observed at the surface. The profile of the atomic concentrations with respect to sputter time is shown in figure A.21.

In this case, the concentration of the oxygen found at the near surface ('no-sputter) is higher and goes deeper than the one observed in the as-nitrided coupon. As the sputtering time increased, the presence of a type of chromium, nitrogen and different 'flavor' of oxygen also increased. This 'sputter' oxygen had a higher atomic concentration than the nitrogen; and at the same time, this oxygen concentration was considerably higher than that observed for the as-nitrided case. Preliminary XPS analysis on the polarized coupon held at 750 mV(SHE) also showed this increased oxygen concentration; and even though the atomic concentration was lower that the one held at 1000 mV(SHE), it was still higher that the nitrogen concentration.

The evolution of the oxygen, nitrogen and chromium peaks for this coupon is shown in figure A.22. Similar to the "as nitrided" coupon, the oxygen found at the surface was different to the one observed after sputtering. In the case of nitrogen and chromium, the first survey had a considerably weak signal for these two elements. However, later in sputtering, the chromium peak started to show and during this process it slightly shifted to the right. In the case of nitrogen the peak seemed to not change position during the surveys.

The shift of the peak positions and the difference in width observed when chromium peaks of the as-nitrided and the polarized surfaces (after sputtering) are compared using a normalized intensity (Figure A.23) demonstrate that in the polarized case the chromium is in a more oxidized state than when no polarization had taken place. However, this "as nitrided" chromium is shifted and wider than the standard for metallic chromium (Figure A.24), which indicates that it is also in a more oxidized state.

The depth reached during the sputtering was estimated to be no more than 100 nm; more likely to be considerably less since the inspection of the surface after sputtering by backscattered SEM did not show any change. This suggests that the data collected was at the very outer surface of the coupon, and the nitrogen found is probably associated with the presence of CrN.

The information obtained from this analysis can be interpreted as shown in Figure A.25, which presents a schematic of the cross sectional view of both coupons. At this point it is possible to suggest that at least one of the causes of the measured currents is related with the oxygen incorporation into/at the nitride layer. However, the exact form of this incorporation (oxide or oxynitride) remains to be determined.

CHAPTER 6
CONCLUSIONS

The final results of this research have resulted in a better understanding of the corrosion properties of chromium nitrides and their benefits and limitations as materials for bipolar plate applications in PEM fuel cells.

1. The nitrided nickel-chromium and nickel-titanium systems were the only ones of a series of model alloys with additions of Ni-X (X=Cr, Nb, Ti,V) that provided a corrosion resistance within the selection criteria established at the beginning of the research (current densities of $1x10^{-6}$ A/cm^2 or less at potentials on the order of 900 – 950 mV (SHE)). However, the TiN coating obtained for the nickel-titanium alloy showed evidence of attack after testing.
2. In a pure nitrogen atmosphere, nitridation temperature and time had a significant effect on the corrosion behavior of the coating obtained. In fact, corrosion protection seemed to increase with increasing nitridation temperature for the Ni-50Cr (wt%) alloys. No evidence of local corrosion attack was observed on any the coated coupons when tested under aerated conditions.
3. The best corrosion resistance under an aerated sulfuric acid electrolyte pH 3 at 80 °C was given by the Ni-50Cr alloy nitrided at 1100 °C for 1-2h in a pure nitrogen atmosphere.
4. Reduction of corrosion protection under aerated conditions was observed when the chromium concentration of the binary Ni-50Cr alloy was reduced, as well as when the nitrogen partial pressure was decreased for the nitridation treatment. These effects were found to be a related to the different microstructures obtained. In all cases, higher corrosion resistance was associated with a mixture of CrN+Cr_2N at the surface in contact with the electrolyte; similarly, in the case of lower protection this microstructure consisted on a mixture of Cr_2N+π phase. The fact that an exclusive, continuous, single-phase layer of the nitrides was not formed precludes a conclusive statement about the inherent corrosion resistance of the individual nitrides under the conditions examined.
5. Nitridation/corrosion/microstructure correlations were primarily studied for the aerated electrolyte.
6. Under anodic environment simulation (hydrogen purged), both surfaces, CrN+Cr_2N and Cr_2N+π phase, showed low corrosion currents.
7. Initial XPS results performed on an "as nitrided" Ni-50Cr coupon (1100 °C, 2h, N_2), as well as on polarized nitrided Ni-50Cr coupons, appear to indicate that at least a part the anodic current densities measured during polarization is related with the incorporation of oxygen into the nitrided surface. The amount of oxygen incorporated seems to increase with the polarization potential. However, the exact form of this incorporation (oxide or oxynitride) is still to be determined.

Finally, although outside the scope of this thesis, results of a 4000 h corrosion test under simulated anodic and cathodic bipolar plate conditions and a 1000 h fuel cell test operated at 0.7 V(SHE) indicated that the 1100 °C, 1-2 h nitrided Ni-50Cr exhibited extremely low levels of metal ion dissolution and negligible increase in contact resistance such that the material appears very promising for PEM fuel cell bipolar plate applications[41].

CHAPTER 7
FURTHER RESEARCH

In terms of the corrosion properties of the chromium nitrides, efforts should be directed to obtaining a single, stable and uniform phase at the surface in contact with the electrolyte. One way to obtain single chromium nitride phase can be by removing the outer phase of one of the already known structures. A Cr_2N single phase can be obtained by grinding the outer CrN phase on the Ni-50Cr coupon nitrided in a pure nitrogen atmosphere for 2 hours at 1100 °C. Once the single phase is obtained a standard polarization test in aerated sulfuric acid (pH 3 and 80 °C) should be performed in order to obtain comparable results.

Better understanding of the source of corrosion currents and corrosion mechanisms of the nitrided Ni-50Cr system is needed. It was determined that oxygen is being incorporated into the system; however, at this point it is not possible to conclude if it is related with the formation of oxides or oxynitrides. XPS studies of pure chromium should be performed in order to obtain information about its natural corrosion behavior under the same conditions at which the nitrides were tested; this will help to identify the characteristic 'flavor' of the species related with the corrosion of chromium. A Ni-50Cr coupon is not suggested because the presence of nickel may affect the results since no nickel has been found on the previous XPS surveys. The polarization should include the standard screening in sulfuric acid pH 3 at 80 °C until 1000 mV(SHE) and then a hold at 1000 mV(SHE) for 5 hours. An additional coupon with the same procedure but holding it at 750 mV(SHE) can also be useful for determining if there is a trend on the spectrum behavior.

Analyses of the electrolytes after the polarization screenings in order obtain information about possible material dissolution into the solution are also suggested.

XPS analyses of the coupons tested in the Ar-4H_2 purged electrolyte (simulating the anode environment) to identify the differences in the nature of the corrosion products and mechanisms in comparison with the aerated electrolyte (cathode environment) will be useful at the moment to establish a more conclusive statement on the behavior of chromium nitrides in sulfuric acid solutions.

Finally, in terms of fuel-cell commercialization and the selection of an efficient bipolar plate material, the Ni-50Cr was studied as a model alloy. Compositions with lower Cr and Ni/Fe bases will be needed to achieve cost targets and commercial viability. The 1100° C nitrided Ni-35Cr and Ni-45Cr alloys were not as corrosion resistant as the nitrided Ni-50Cr. Modification of the nitridation conditions, in combination with alloying additions, should be pursued to improve the protective quality of the nitride formed on these lower Cr alloys, ideally with a goal of Cr levels less than 25-30 wt.% and the use of Fe-base or Ni/Fe base alloys.

REFERENCES

1. Brian, C. and Heinzel A. "Materials for Fuel Cell Technologies" in Nature. 2001; 414: 345-352.
2. Borup, R. and Vanderborgh N. "Design and Testing Criteria for Bipolar Plate Materials for PEM Fuel Cell Application" in Materials for Electrochemical Energy, Storage and Conversion. MRS. 1995; 393: 151-235.
3. Tjokro, K. and Young, D. "Comparison of internal Nitridation Reactions in Ammonia and Nitrogen" in Oxidation of Metals. 1995; 44: 453-475. ISSN: 0030-770X.
4. Besmann, T.; Klett, J.; Henry J. and Lara-Curzio, E. "Carbon/Carbon Composite Bipolar Plate For Proton Exchange Membrane Fuel Cells" in Journal of Electrochemical Society. 2000; 147: 4083-4086. ISSN: 0013-4651.
5. Adcock, P.; Davies, D.; Turpin, M. and Rowen, S. "Stainless Steel as a Bipolar Plate Material for Solid Polymer Fuel Cells" in Journal of Power Sources. 2000; 86: 237-242. ISSN: 0378-7753.
6. Makkus R.; Janssen, A.; De Bruijn, F. and Mallant, R. "Use of Stainless Steel for Cost Competitive Bipolar Plates in SPFC" in Journal of Power Sources. 2000; 86: 274-282. ISSN: 0378-7753.
7. Uchida H.; Inoue, S. and Koterazawa K. "Electrochemical Evaluation if Pinhole Defects in TiN Films Prepared by r.f. Reactive Sputtering" in Materials Science and Engineering. 1997: 649-652. ISSN: 0921-5093.
8. Franco, C.V.; Fontana L.C.; Bechi, D.; Martinelli A.E. and Muzart R. "An Electrochemical Study of Magnetron-Sputtered Ti- and TiN-Coated Steel" in Corrosion Science. 1998; 40: 103-112. ISSN:0010-938X.
9. Brady, M.P.; Weisbrod, K.; Zawodzinski, C.; Paulauskas, I.; Buchanan, R.A. and Walker, L. "Assessment of Thermal Nitridation to Protect Metal Bipolar Plates in PEM Fuel Cells" in Journal of Electrochemical and Solid State Letters.
10. Ziegler P.F. and Rausch J.J. in Surface and Coating Technology. 1986; 29: 259
11. Krupp, U.; Chang, S. and Christ H. "Occurrence of the Ternary π Phase during Nitriding of Ni-Cr and Ni-Cr-Ti Alloys and its Thermodynamic Prediction" in ?. 2000; . ISSN: 0044-3093.
12. Thomas S. and Zalbowitz M. Fuel Cells: Green Power. Los Alamos National Laboratory.
13. Hodgson, D.; May, B.; Adcock, P. and Davies, D. "New Lightweight Bipolar Plate System for Polymer Electrolyte Membrane Fuel Cell" in Journal of Power Sources. 2001; 96: 233-235. ISSN: 0378-7753.
14. Prater, K. "Polymer Electrolyte Fuel Cells:A Review of Recent Developments" in Journal of Power Sources. 1994; 51:129-144. ISSN: 0378-7753.
15. Barbir, F. and Gomez, T. "Efficiency and Economics of Proton Exchange Membranes (PEM) Fuel Cells" in Int. J. Hydrogen Energy. 1996; 10: 891-901. ISSN: 0360-3199.
16. Hirschenhofer, J., Stauffer D. and Engleman R. Fuel Cells: A Handbook (Revision 3). U.S. Department of Energy. 1994
17. Rutttinger, W,; Ilinich, O. and Farrauto R. "A New Generation of water Gas Shift for Fuel Cell Applications" in Journal of Power Sources. 2003; 118: 61-65. ISSN: 3878-7753.

18. Alberti, G. and Casciola, M. "Solid State Protonic Conductors, Present Main Applications and Future Prospects" in Solid State Ionics. 2001; 145:3-16. ISSN: 0167-2738.
19. Dupont™. Nafion® PESA Membranes. Product Information
20. Liu, W.; Ruth, K. and Rusch, G. "Membrane Durability in PEM Fuel Cells" in Journal of New Materials for Electrochemical Systems. 2001; 4: 227-231.
21. Corrosion, Understanding the Basics. 1st Edition. ASM International. 2000. ISBN: 0-87170-641-5
22. Ma, L.; Watrthesen S.; and Shores, D. "Evaluation of Materials for Bipolar Plates in PEMFCs" in Journal of New Materials for Electrochemical Systems. 2000: 221-228.
23. Hentall P.; Lakeman J.; Mepsted G. and Adcock P. "New Materials for Polymer Electrolyte Membrane Fuel Cell Current Collectors" in Journal of Power Sources. 1999; 80: 235-241. ISSN: 0378-7753
24. Kimble, M.C.; Woodman A.S. and Anderson, E.B. "Characterization of Corrosion-Protective Methods for Electrically Conductive Coatings on Aluminum" in American Electroplater and Surface Finishers Society (AESF SUR/FIN '99 Proceedings). 1999; 6: 21-24.
25. Stansbury, E. and Buchanan, R. Fundamentals of Electrochemical Corrosion. 1st Edition. ASM International. ISBN: 0-87170-676-8.
26. Betteridge W. Nickel and its Alloys. 1st Edition. Ellis Horwood Limited. 1984. ISBN: 0-85312-729-7.
27. Brady M.P.; Gleeson, B. and Wright I. in "Alloy Design Strategies for Promoting Protective Oxide-Scale Formation" in Journal of The Minerals, Metals & Materials Society. 2000; 52: 16-21.
28. Briks, N. and Meier, G. Introduction to High Temperature Oxidation of Metals. 1st Edition. Edward Arnold. 1983. ISBN: 0-7131-3464-X.
29. Fromhold, A.T. Theory of Metal Oxidation. Volume I – Fundamentals. 1st Edition. 1976. North-Holland Publishing Company. ISBN: 0-7204-1759-7.
30. Hauffe, K. Oxidation of Metals. Plenum Press. 1965.
31. Krupp, U.; Christ, H. "Internal Nitridation of Nickel-Base Alloys of the Ni-Cr-Al-Ti System" in Oxidation of Metals. 1999; 52: 227-320. ISSN:0030-770X.
32. Kodentonv, A.; Glupen, C.; Cserhati, C.; Kivilathi, J.and Van Loo, F. "High Temperature Nitridation of Ni-Cr Alloys in Metallurgical and Materials Transactions. 1996; 27A: 59-69.
33. Rubly, R. and Douglass D. "Internal Nitridation of Nickel-Chromium Alloys" in Oxidation of Metals. 1991; 35: 259-278. ISSN: 0400-0259.
34. Buijnsters, J.G.; Shankar, P.; Sietsma, J. and ter Muelen, J.J. "Gas Nitriding of Chromium in NH_3-N_2 Atmosphere" in Materials Science and Engineering. 2002; A341: 289-295. ISSN: 0921-5093.
35. Zenghu H.; Jiawan, T.; Quiaxi, L.; Xiaojiang, Y. and Geyang, L. "Effect of N_2 Partial Pressure on the Microstructure and Mechanical Properties of Magnetron Sputter CrNX Films" in Surface and Coating Technology. 2002; 162: 189-193. ISSN: 0257-8972.

36. Zhou, Q.G.; Bai, X.D.; Chen, X.W.; Peng D.Q.; Ling Y.H. and Wang, D.R. "Corrosion Resistance of Duplex and Gradient CrNx coated H13 Steel" in Applied Surface Science. 2003; Article in Press: 1-7. ISSN: 0169-4332.
37. Taguchi, M. and Kurihara, J. "Effect of Surface Nitridation on Corrosion Resistance of Chromium in Sulfuric Acid Solutions" in Materials Transactions. 1991; 32: 1170-1176. ISSN: 0021-4876
38. Taguchi, M. and Takahashi H. "Corrosion Behavior of Chromium Nitride Films Produced by Reactive Ion Plating in Sulfuric Acid Solutions" in Materials Transactions. 1994; 35: 356-362. ISSN: 0916-1821.
39. Bertrand G.; Mahdjoub, H. and Meunier C. "A Study of the Corrosion Behavior and Protective Quality of Sputtered Chromium Nitride Coatings" in Surface and Coatings Technology. 2000; 126: 199-209. ISSN: 0257-8972.
40. Chang, H.; Koschany, P.; Lim, C. and Kim, J. "Materials and Processes for Light Weight and High Power Density Fuel Cells" in Journal of New Materials for Electrochemical Systems. 2000; 3:55-59.
41. Brady, M.; Weisbrod, K.; Paulauskas, I.; Buchanan, R.; More, K.; Wang, H.; Wilson. M.; Garzon, F.; Walker, L. "Preferential Thermal Nitridation to Form Defect-Free Nitride Surface Layers" in Scripta Materialia (in press).

APPENDIX

Table A.1. Comparison of Five Fuel Cell Technologies			
Fuel Cell	Electrolyte	Operating T (°C)	Electrochemical Reactions
PEM	Solid organic polymer poly-perfluorosulfonic acid	60 – 100	Anode: $H_2 \rightarrow 2H^+ + 2e^-$ Cathode: $\frac{1}{2} O_2 + 2H^+ + 2e^- \rightarrow H_2O$ Cell: $H_2 + \frac{1}{2} O_2 \rightarrow H_2O$
AFC	Aqueous solution of potassium hydroxide soaked in a matrix	90 – 100	Anode: $H_2 + 2(OH)^- \rightarrow 2H_2O + 2e^-$ Cathode: $\frac{1}{2} O_2 + H_2O + 2e^- \rightarrow 2(OH)^-$ Cell: $H_2 + \frac{1}{2} O_2 \rightarrow H_2O$
PAFC	Liquid phosphoric acid soaked in a matrix	175 – 200	Anode: $H_2 \rightarrow 2H^+ + 2e^-$ Cathode: $\frac{1}{2} O_2 + 2H^+ + 2e^- \rightarrow H_2O$ Cell: $H_2 + \frac{1}{2} O_2 \rightarrow H_2O$
MCFC	Liquid solution of lithium, sodium and/or potassium carbonates in a matrix	600 – 1000	Anode: $H_2 + CO_3^{2-} \rightarrow H_2O + CO_2 + 2e^-$ Cathode: $\frac{1}{2} O_2 + CO_2 + 2e^- \rightarrow CO_3^{2-}$ Cell: $H_2 + \frac{1}{2} O_2 + CO_2 \rightarrow H_2O + CO_2$ (CO_2 is consumed at cathode and produced at anode)
SOFC	Solid zirconium oxide to which a small amount of ytrria is added	600 – 1000	Anode: $H_2 + O^{2-} \rightarrow H_2O + 2e^-$ Cathode: $\frac{1}{2} O_2 + 2e^- \rightarrow O^{2-}$ Cell: $H_2 + \frac{1}{2} O_2 \rightarrow H_2O$

From: Fuel Cells – Green Power. By: S. Thomas and M. Zalbowitz. LANL

Where:

H_2: Hydrogen
H^+: Hydrogen Ion
e-: Electron
O_2: Oxygen
H_2O: Water
OH^-: Hydroxyl Ion
CO: Carbon Monoxide
CO_2: Carbon Dioxide
CO_3^{2-}: Carbonate Ion

Table A.2. PEM Fuel Cell Operating Conditions for Bipolar Plate Materials Design	
Temperature	70 – 100 °C
Pressure	2 – 3 atm
Anode Potential (long term)	0.1 V (SHE)
Anode Potential (peak)	0.6V(SHE)
Anode Water pH	3.60
Anode Fluoride Concentration	1.8 ppm
Anode Environment	Reducing (H_2)
Cathode Potential (long term)	0.8 V(SHE)
Cathode Potential (peak)	1.23 V(SHE)*
Cathode Water pH	4.02
Cathode Fluoride Concentration	1.1ppm
Cathode Environment	Oxidizing (O_2)

* This ideal value may change depending on some variables, such as, local crossover or internal current at open circuit. In real operating conditions, this value tends to be around 0.9-0.95V (SHE).

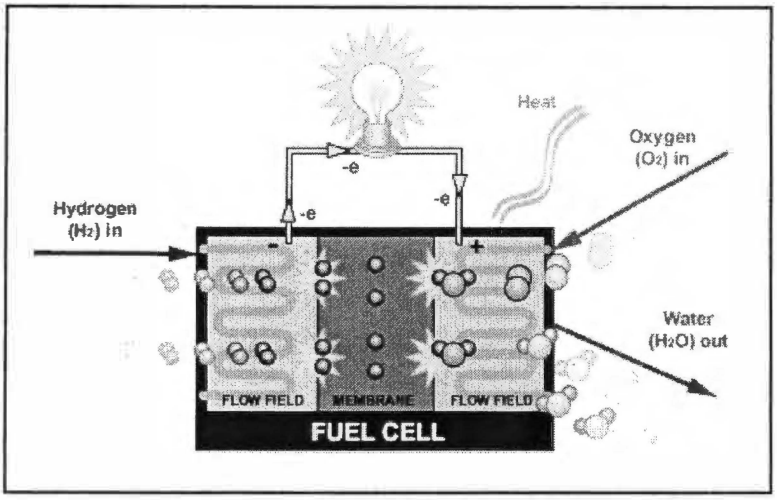
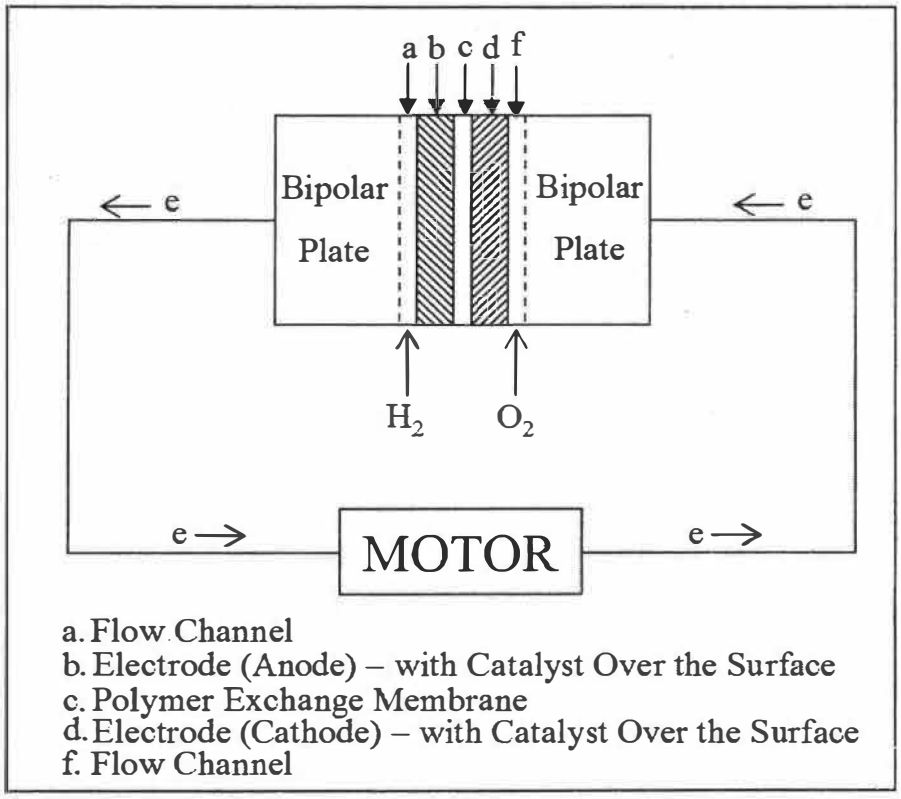


Figure A.1. Fuel Cell Basic Operation.
From: http://www.hpower.com/pem.shtml



A.2. Schematic Diagram Showing the Components of a Polymer Electrolyte Membrane Fuel Cell. From: R.A. Buchanan.

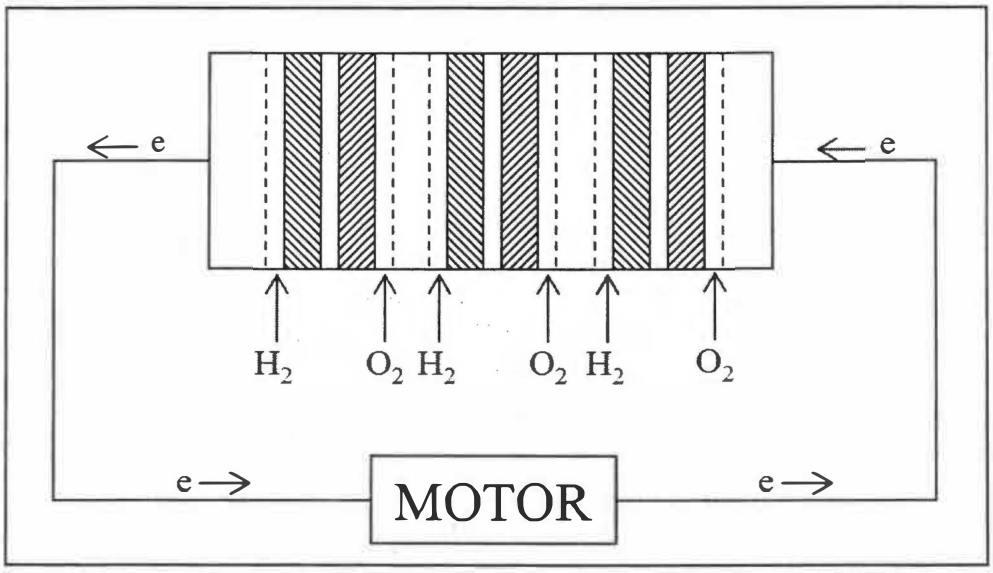


Figure A.3. Schematic Diagram of Three Polymer Electrolyte Membrane Fuel Cells Stacked in Series. See Figure A.2 for Components Identifications. From: R.A. Buchanan.

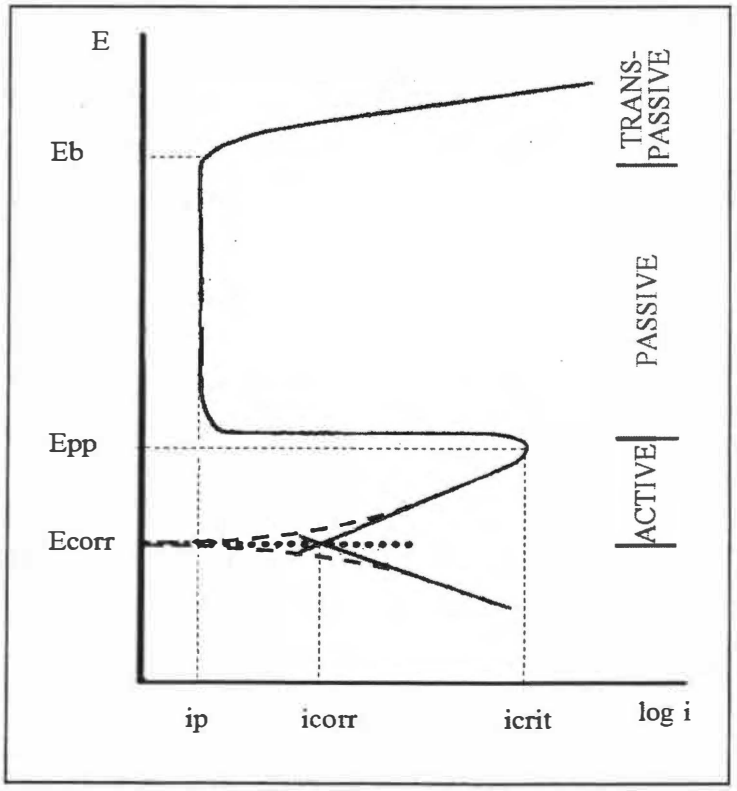
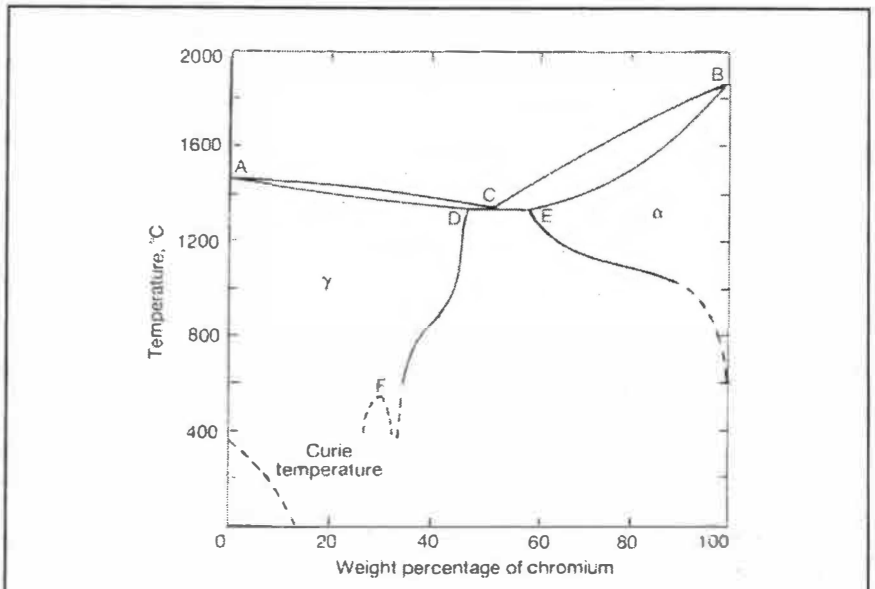


Figure A.4. Anodic Polarization Curve of an Active-Passive Material. Adapted from: E. E. Stansburry and R. A Buchanan. Fundamentals of Electrochemical Corrosion.



Point	A	B	C	D	E	F
°C	1453	1880	1345	1345	1345	580
%wt	0	100	51	47	59	31

Figure A.5. Nickel Chromium Phase Equilibrium Diagram.
From: W. Betteridge. Nickel and its Alloys.

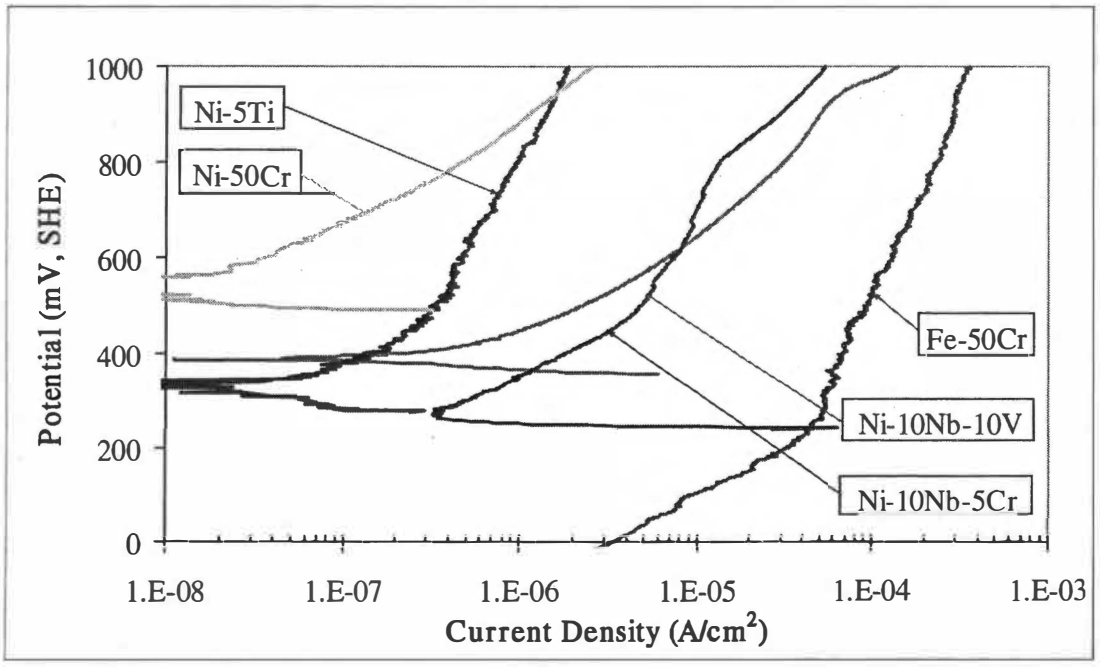


Figure A.6. Anodic Polarization Curves of Different Nitrided Alloys.

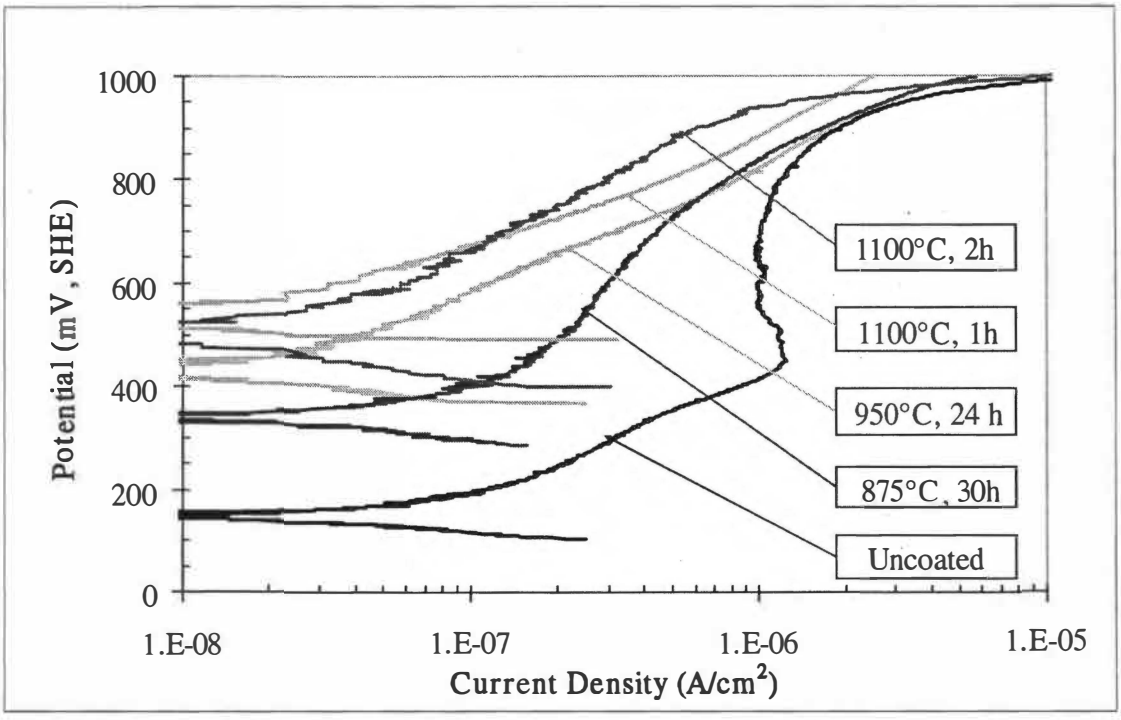


Figure A.7. Ni-50Cr Anodic Polarization Curves. Effect of Temperature and Timing on Nitridation in a Pure Nitrogen Atmosphere.

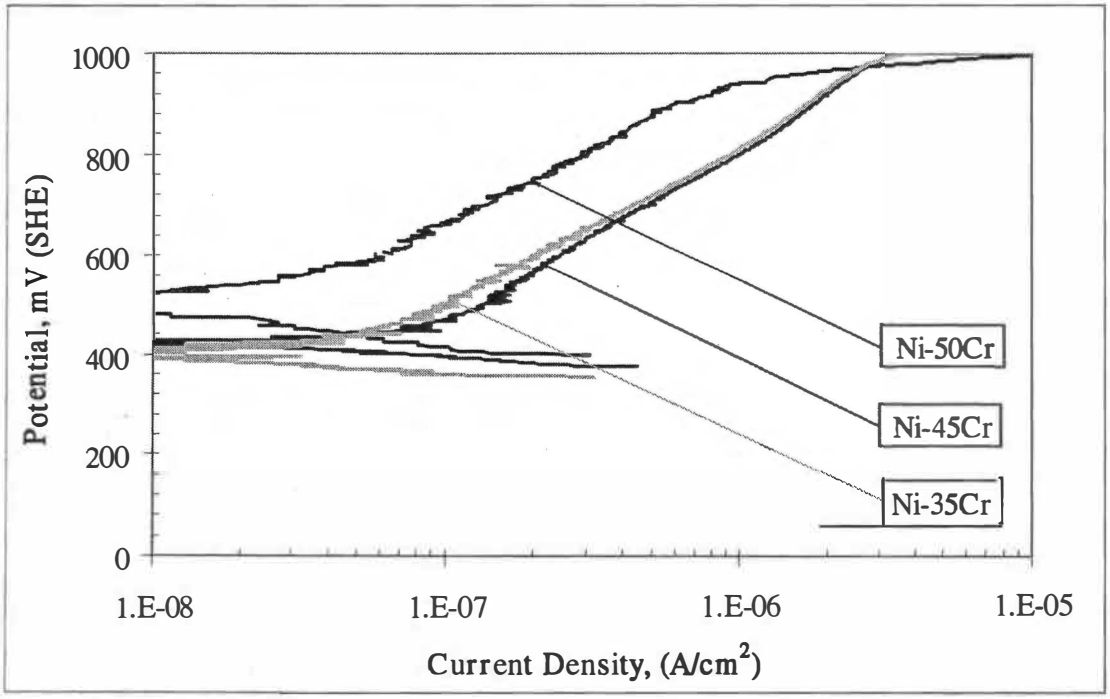


Figure A.8. Effect of Alloy Composition on Nitridation at 1100 °C for 2 h in a Pure Nitrogen Atmosphere.

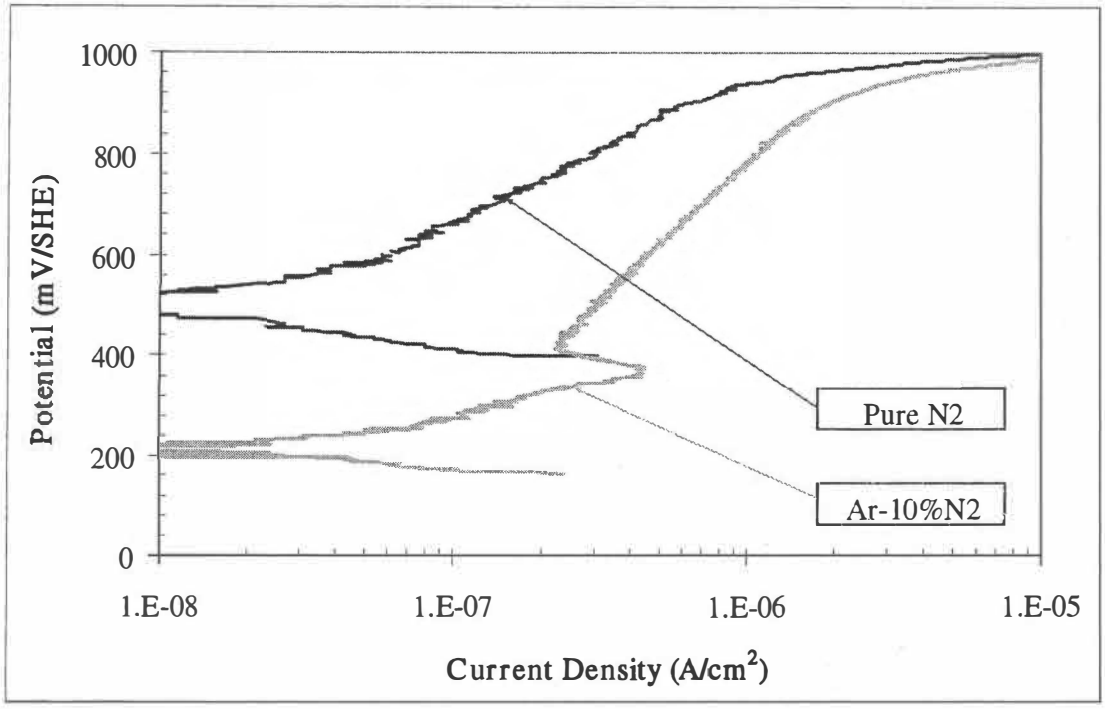


Figure A.9. Effect of the Nitrogen Partial Pressure. Ni-50Cr Anodic Polarization Curves. Pure Nitrogen and Ar-10%N_2 at 1100 °C for 2 h.

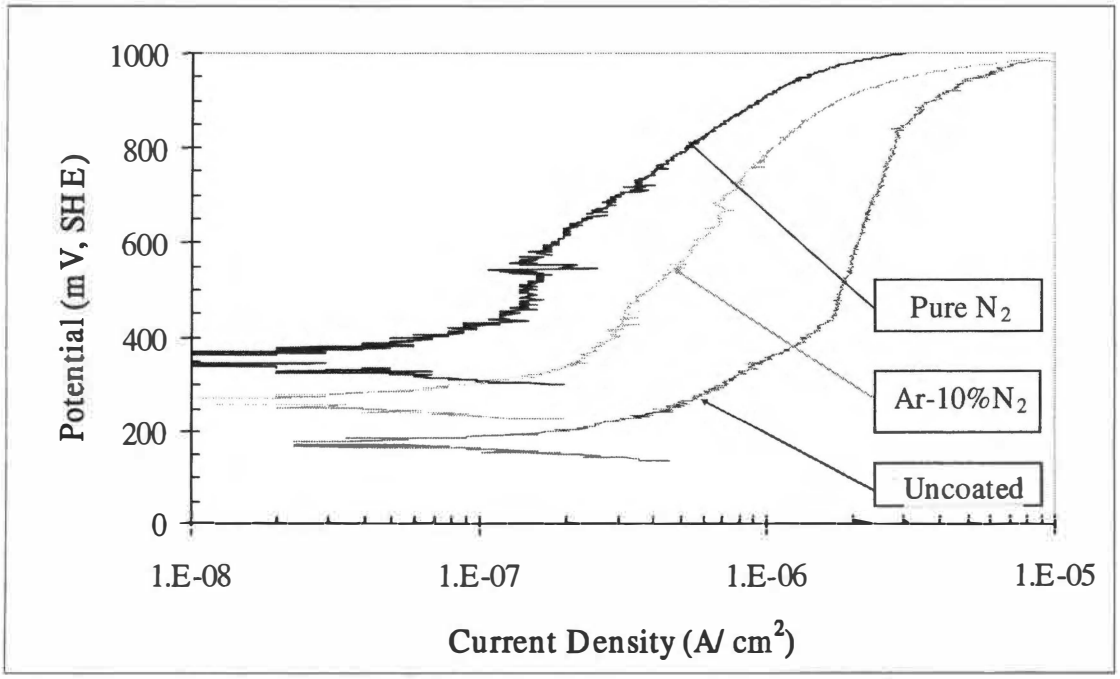


Figure A.10. Polarization Curves of Pure Chromium. Uncoated and Nitrided at 1100 °C for 2h.

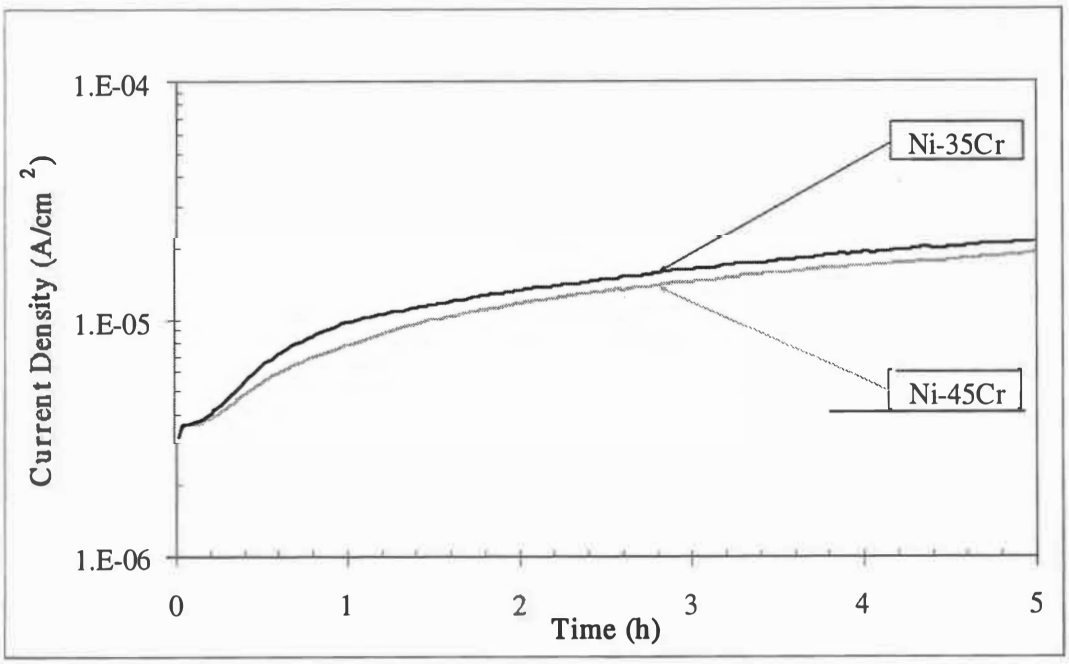


Figure A.11. Protective Quality at 1000 mV (SHE) for the Ni-35Cr and Ni-45Cr Nitrided at 1100 °C for 2 h in Pure Nitrogen.

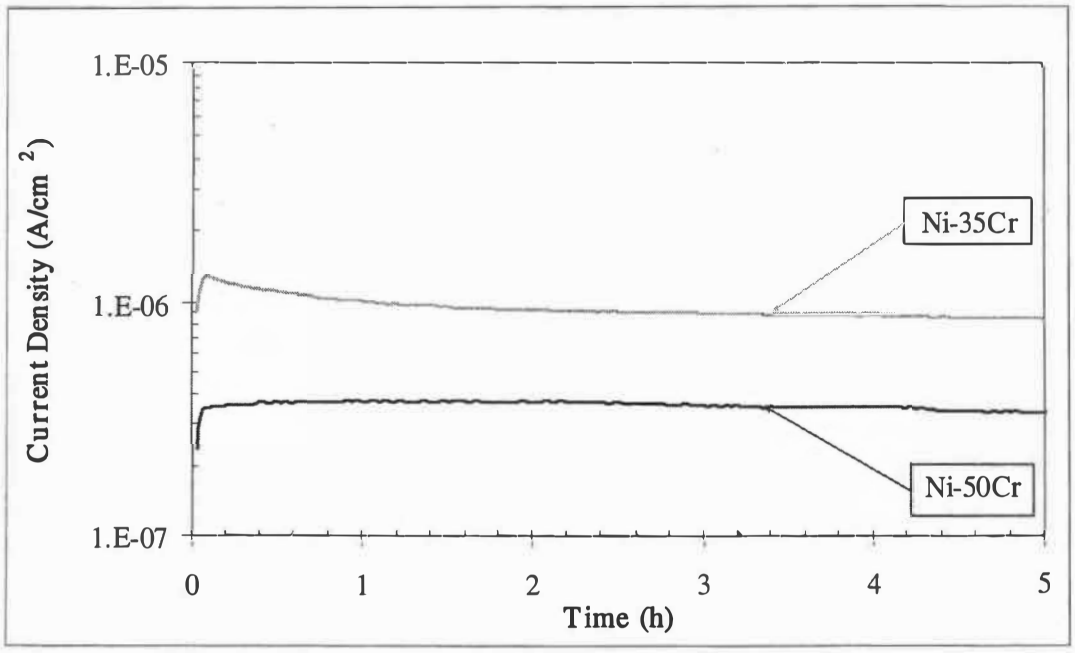


Figure A.12. Protective Quality at 750 mV (SHE) for the Ni-35Cr and Ni-50Cr Nitrided at 1100 °C for 1 h in Pure Nitrogen.

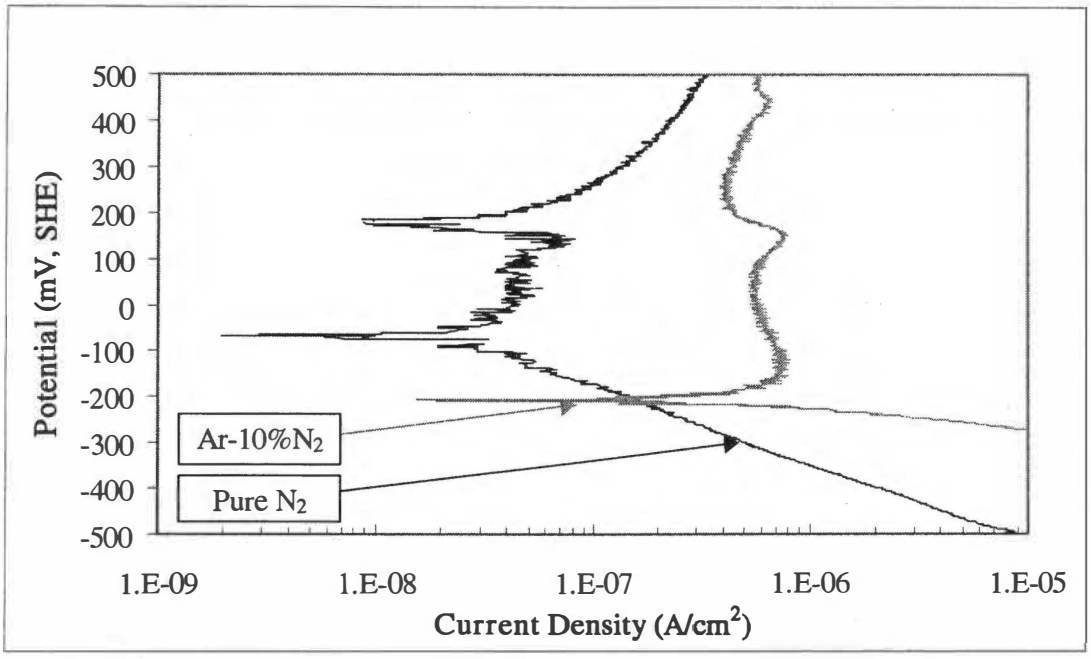


Figure A.13. Polarization Curves in Deaerated Electrolyte of Nitrided Ni-50Cr Alloys at 1100 °C in Pure N_2 and Ar-10%N_2 for 2 h and 5 h Respectively.

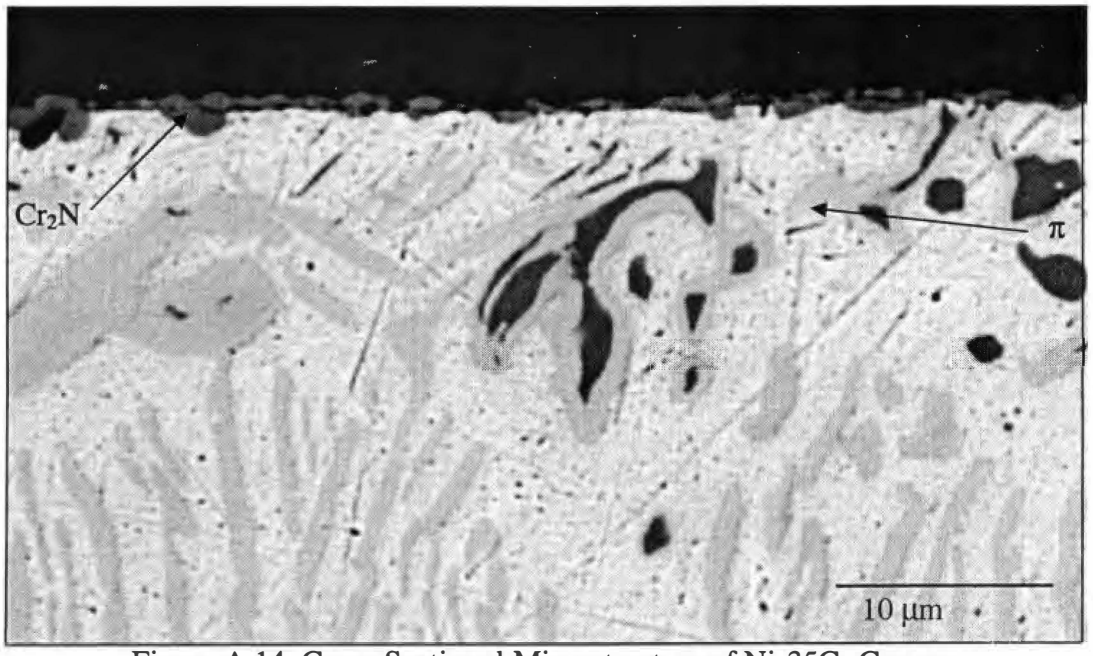


Figure A.14. Cross Sectional Microstructure of Ni-35Cr Coupon Nitrided at 1100 °C for 2 h in Pure Nitrogen.

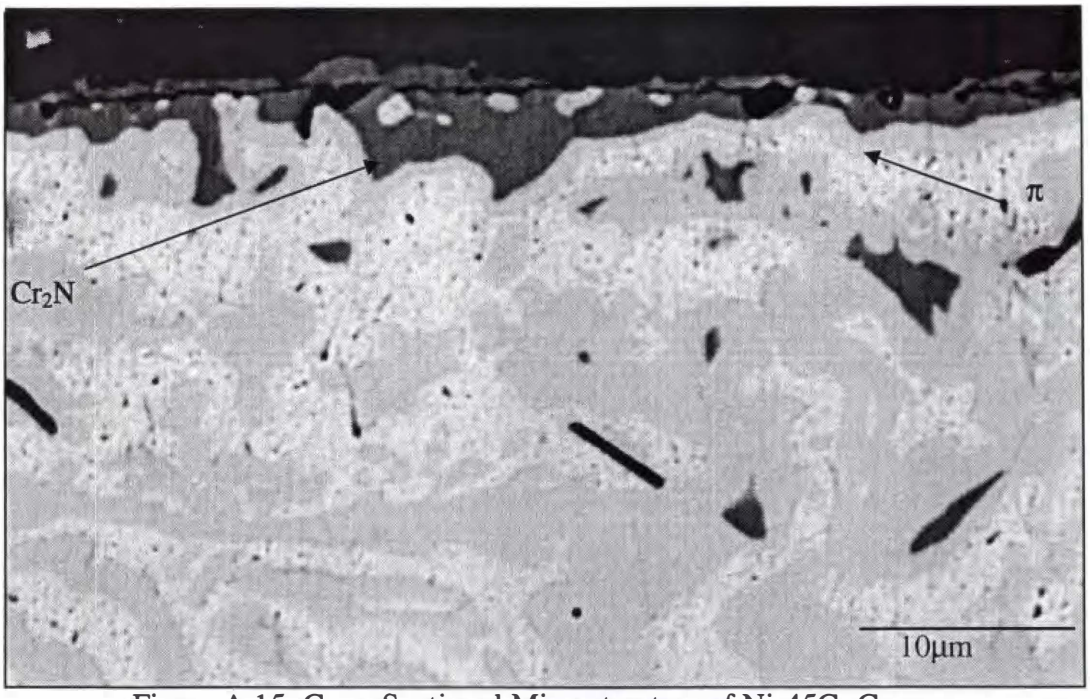


Figure A.15. Cross Sectional Microstructure of Ni-45Cr Coupon Nitrided at 1100 °C for 2 h in Pure Nitrogen.

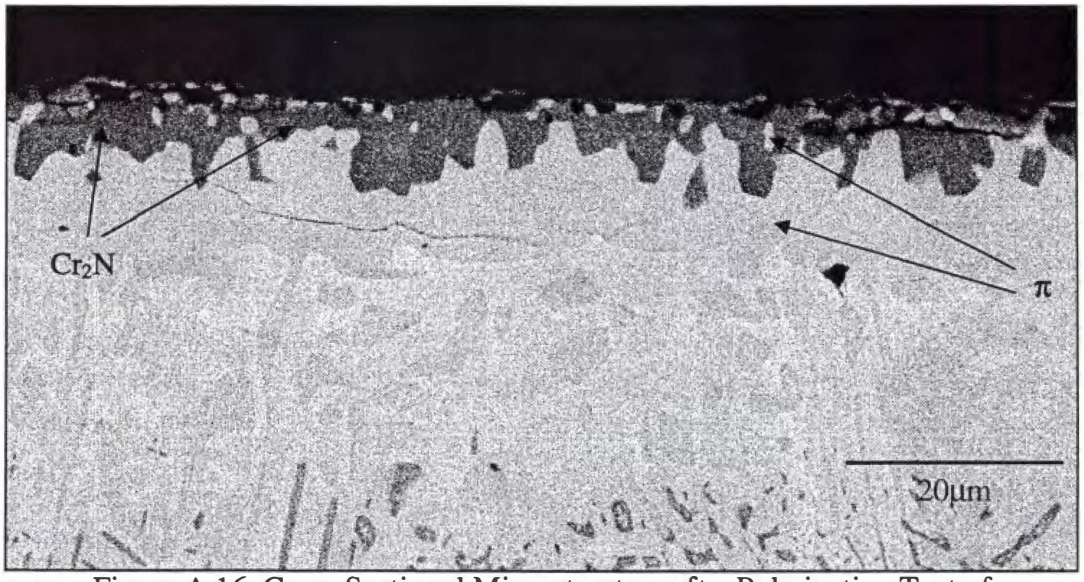


Figure A.16. Cross Sectional Microstructure after Polarization Test of Ni-50Cr Coupon Nitrided at 875 °C for 30 h in Pure Nitrogen.

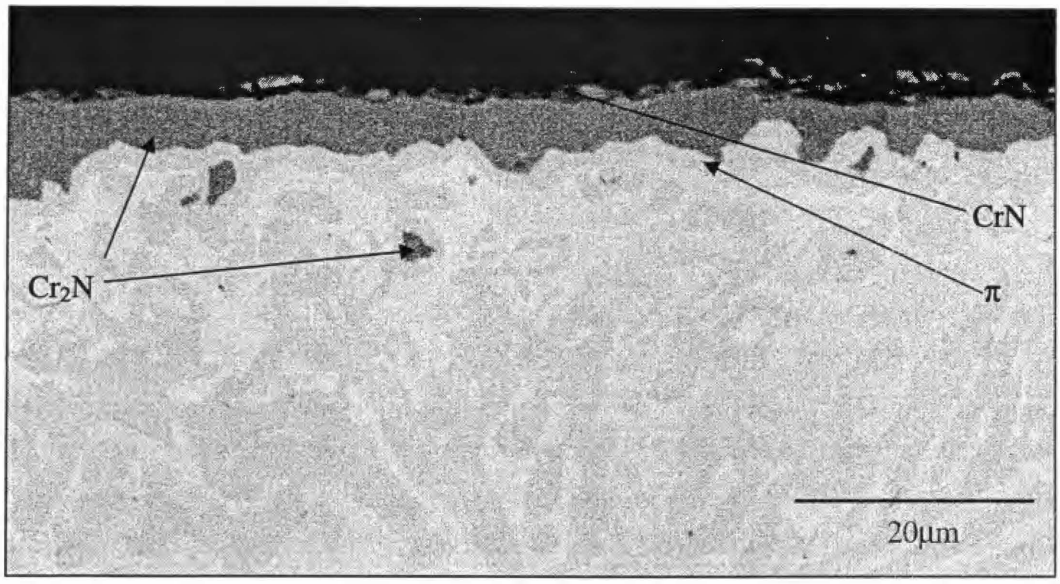


Figure A.17. Cross Sectional Microstructure after Polarization Test of Ni-50Cr Coupon Nitrided at 1100 °C for 1 h in pure Nitrogen.

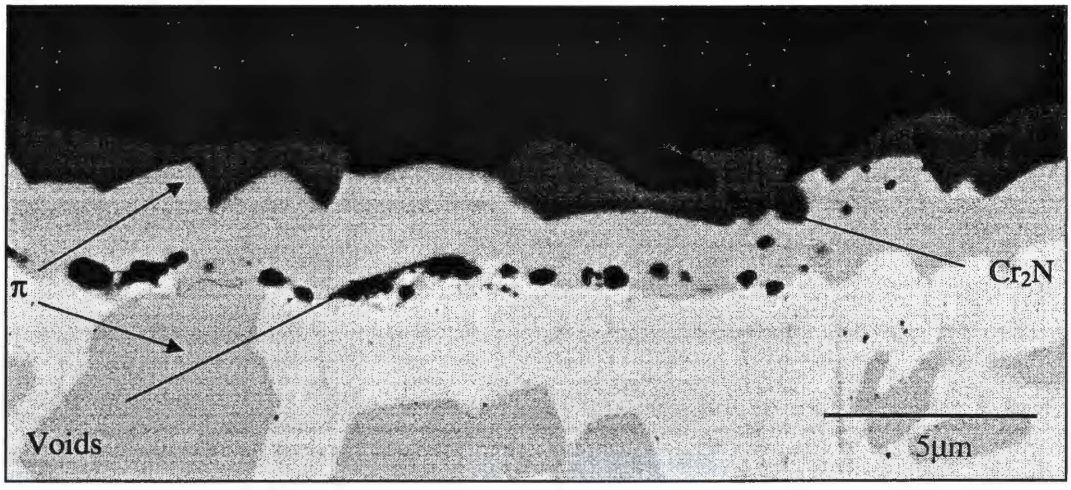


Figure A.18. Cross Sectional Microstructure after Polarization Test of Ni-50Cr Coupon Nitrided at 1100 °C for 2 h in Ar-10%N_2.

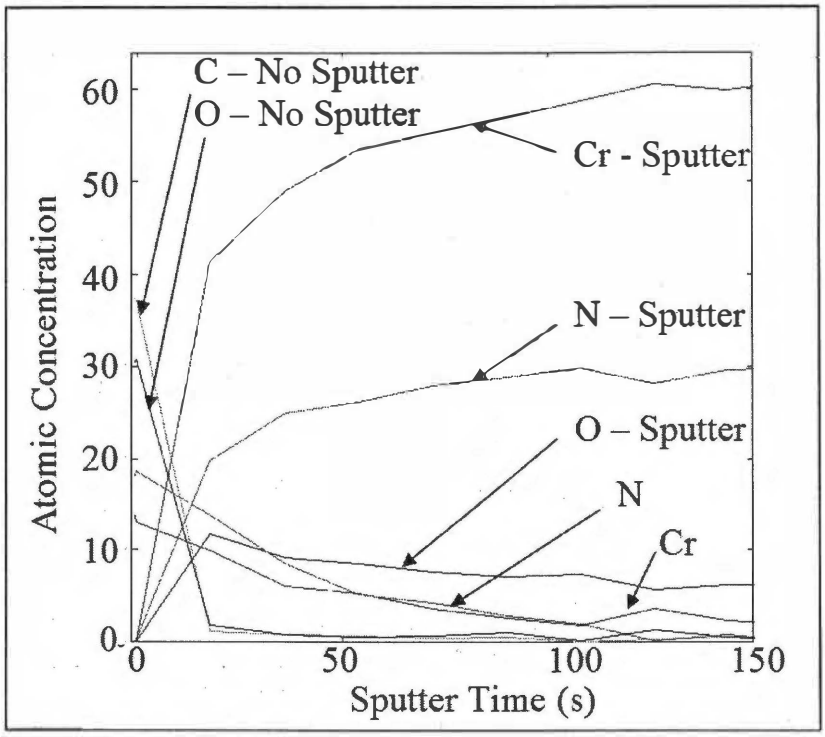
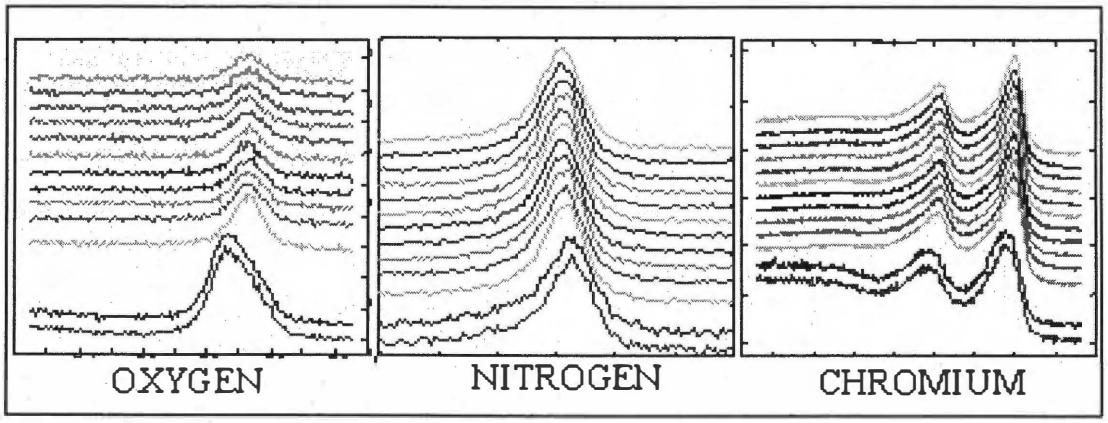


Figure A.19. Concentration Profile of Ni-50Cr Coupon Surface Nitrided at 1100 °C for 2 h in Pure N_2, without Polarization Testing ("as nitrided").



A.20. Evolution of the Oxygen, Nitrogen and Chromium Peaks Throughout Sputter of "as nitrided" Ni-50Cr Coupon.

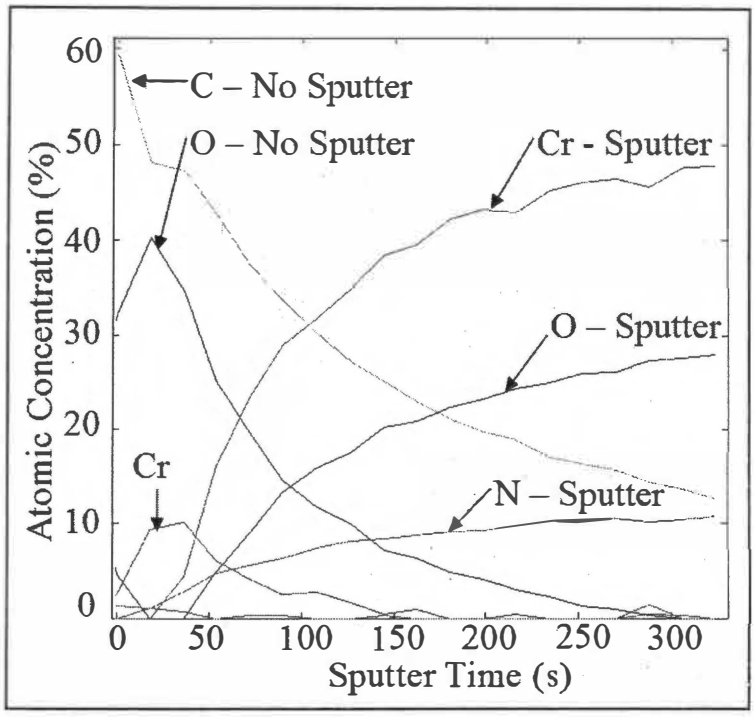
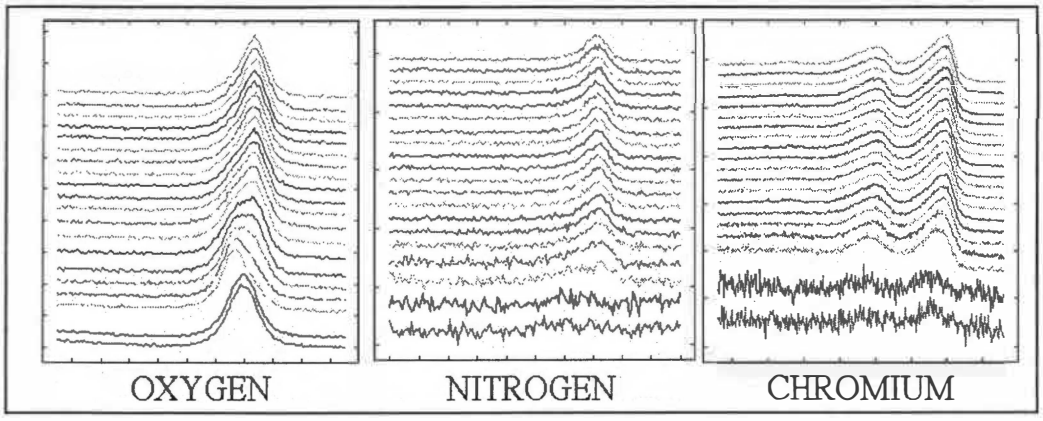


Figure A.21. Concentration Profile of the Polarized Ni-50Cr Coupon Surface (Nitrided at 1100 °C for 2 h in Pure N_2) Hold at 1000 mV(SHE) for 5 h.



A.22. Evolution of the Oxygen, Nitrogen and Chromium Peaks Throughout Sputter of the Polarized Ni-50Cr Coupon Surface (Nitrided at 1100 °C for 2 h in Pure N_2) Hold at 1000 mV(SHE) for 5 h.

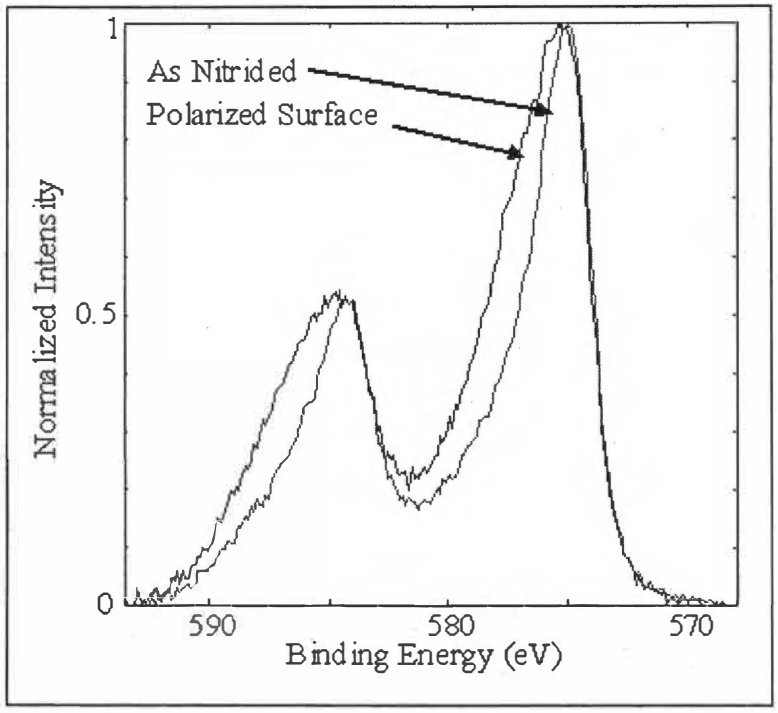


Figure A.23. Comparison of the Chromium Peaks after Final Sputter for the Ni-50Cr Nitrided Coupons (1100 °C, 2 h, N_2) with and without Polarization Testing.

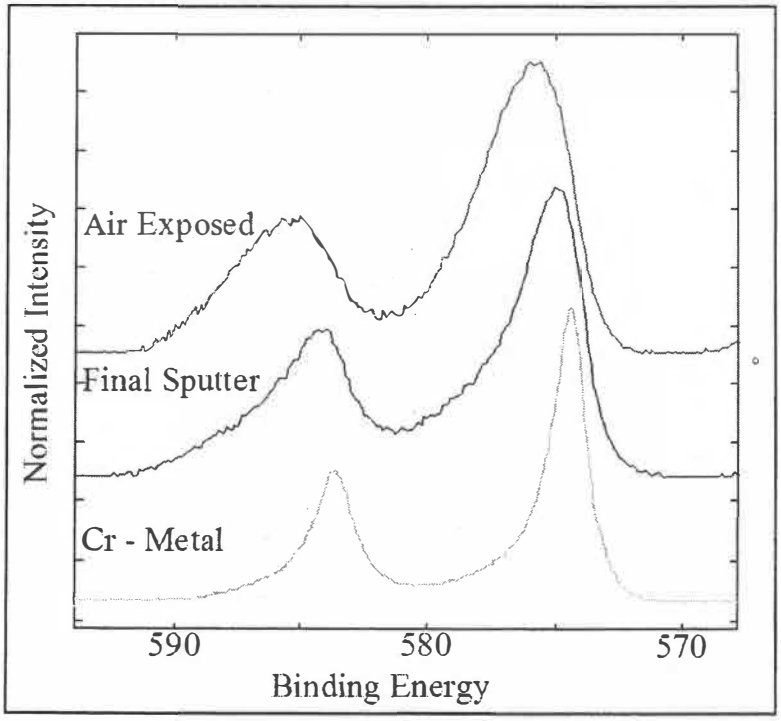


Figure A.24. Comparison of the Chromium Peaks on the "As Nitrided" Case (After Sputter) with the Characteristic Cr Metal Peak.

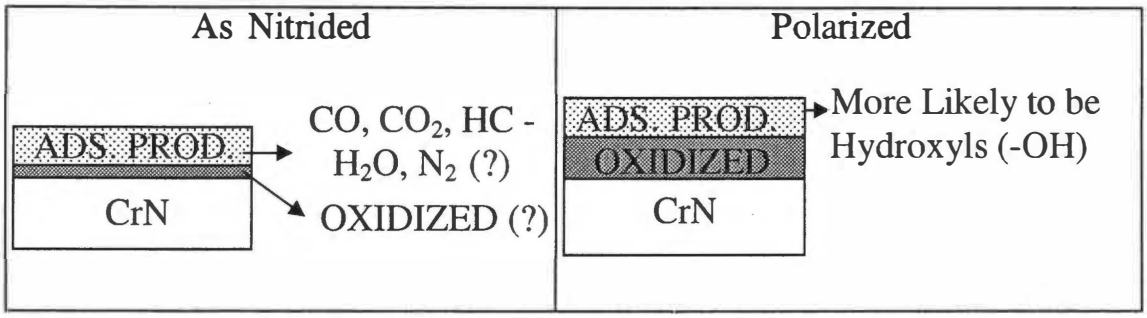


Figure A.25. Schematic Representation of the Cross Sectional Areas of the Ni-50Cr Nitrided Coupons (1100 °C, 2 h, N_2). a. As nitrided case. b. After Polarization Studies.

VITA

Irene Elizabeth Paulauskas Vasaitis was born in Maracaibo, Venezuela on November 13, 1980. She attended to the University Rafael Urdaneta in Maracaibo, Venezuela, and graduated with a Bachelor's of Engineering with a major in chemical engineering in July of 2001. She enrolled in the department of Materials Science and Engineering at the University of Tennessee, Knoxville, in the fall of 2001. In 2003 received a Master of Science in Materials Science and Engineering.

Irene E. Paulauskas is currently pursuing a doctorate in Materials Science and Engineering at the University of Tennessee.

3872 2089 23
04/14/04 MRB